Remote Sensing of Environment xxx (2015) xxx–xxx

Contents lists available at ScienceDirect

Remote Sensing of Environment

journal homepage: www.elsevier.com/locate/rse

Advantages using the thermal infrared (TIR) to detect and quantify semi-arid soil properties

Andreas Eisele [a,*], Sabine Chabrillat [a], Christoph Hecker [b], Robert Hewson [c], Ian C. Lau [d], Christian Rogass [a], Karl Segl [a], Thomas John Cudahy [d], Thomas Udelhoven [e], Patrick Hostert [f], Hermann Kaufmann [a]

[a] Helmholtz Centre Potsdam, German Research Centre for Geosciences, Telegrafenberg, 14473 Potsdam, Germany
[b] Department of Earth Systems Analysis, Faculty of Geo-Information Science and Earth Observation (ITC), University of Twente, Hengelosestraat 99, P.O. Box 217, Enschede 7500AE, The Netherlands
[c] School of Mathematical and Geospatial Sciences, RMIT University, GPO Box 2476, Melbourne, VIC 3001, Australia
[d] CSIRO Mineral Resources Flagship, CSIRO, 26 Dick Perry Avenue, Kensington, WA 6151, Australia
[e] Environmental Remote Sensing and Geoinformatics Department, University of Trier, Behringstr. 15, D-54286 Trier, Germany
[f] Geography Department, Humboldt-Universität zu Berlin, Unter den Linden 6, D-10099 Berlin, Germany

ARTICLE INFO

Article history:
Received 9 October 2014
Received in revised form 28 March 2015
Accepted 3 April 2015
Available online xxxx

Keywords:
Thermal infrared (TIR)
Longwave infrared (LWIR)
Emission FTIR spectroscopy
Digital soil mapping (DSM)
Semi-arid soils
Soil properties
Soil grain coatings
Soil organic carbon (SOC)
Soil texture
Particle size
Topsoil coarsening

ABSTRACT

Monitoring soil surface dynamics in semi-arid agricultural landscapes becomes increasingly important due to the vulnerability of these ecosystems to desertification processes. Observations using remote sensing via the traditionally used visible-near infrared (VNIR) and shortwave infrared (SWIR) wavelength regions can be limited due to the special characteristics of such soils (e.g. rich in quartz, poor in clay minerals, coarse textured, and grain coatings). In this laboratory-based work we demonstrate the capabilities of the thermal infrared between 8 and 14 μm (longwave infrared) to detect and quantify small ranges of the soil properties sand-, clay, and soil organic carbon (SOC) content, as they appear in the semi-arid agricultural landscapes of the Mullewa region in Western Australia. All of the three soil properties could be predicted using the longwave infrared (LWIR) spectra with higher accuracy and precision than from the VNIR-SWIR wavelength region. The study revealed the complex relationships between the soil properties and the VNIR-SWIR soil spectra, which were caused by the spectral influence of the soils' grain coatings (based on iron and clay minerals). These difficulties could be handled more appropriately by the prediction models based on the LWIR soil spectra. Our results indicate that in order to quantitatively monitor farming areas for such erosion-related soil properties; remote sensing using the LWIR wavelength region would produce better estimates than using the wavelength ranges in the VNIR-SWIR.

1. Introduction

Due to the rise in concerns of food security, there is a growing realization for the need to utilize remote sensing for the monitoring of the conditions of soils in agricultural regions. Fertile soils are the basis for global food production, but their distribution is limited and they are increasingly under pressure to produce higher yields. In this context dryland ecosystems have a particularly important role since these areas are responsible for more than 40% of the worldwide food production and are particularly suffering from desertification (UNCCD, 2011). Semi-arid soils contain low content in clay minerals and organic carbon, which generally assist processes of aggregate formation in a soil's matrix and increase surface stability (Brady & Weil, 2008). These soils are particularly prone to maximum wind erosional forces after crop harvesting, when bare soil surfaces are dry. Topsoil texture is closely related to desertification and coarsening of topsoil is an indicator for this process (Xiao, Shen, Tateishi, & Bayaer, 2006). Monitoring the surface dynamics of critical soil properties, such as grain size distribution and organic carbon content, provides farmers with the information to detect soil vulnerable to erosion in its early stages in order to locally intervene.

The quantification of such soil properties through remote sensing data has traditionally been undertaken using the solar reflective spectral wavelength range (visible, VIS: 0.4–0.7 μm; near infrared, NIR: 0.7–1.1 μm; shortwave infrared, SWIR: 1.1–2.5 μm). Remote sensing in the VNIR-SWIR predominantly depends on reflected radiance of the object with the sun as the energy source. In proximal reflectance spectroscopy and imaging spectroscopy, the use of the VNIR-SWIR has already been demonstrated to be beneficial for this purpose (Bartholomeus, Epema, & Schaepman, 2007; Ben-Dor et al., 2008, 2009; Chabrillat, Goetz, Krosley, & Olsen, 2002; Chang & Laird, 2002; Crouvi, Ben-Dor, Beyth, Avigad, & Amit, 2006; Gomez, Viscarra Rossel, & McBratney, 2008;

* Corresponding author. Tel.: +49 331 288 28984; fax: +49 331 288 1192.
E-mail addresses: eisele@gfz-potsdam.de (A. Eisele), chabri@gfz-potsdam.de (S. Chabrillat), c.a.hecker@utwente.nl (C. Hecker), robert.hewson@rmit.edu.au (R. Hewson), Ian.Lau@csiro.au (I.C. Lau), rogass@gfz-potsdam.de (C. Rogass), segl@gfz-potsdam.de (K. Segl), Thomas.Cudahy@csiro.au (T.J. Cudahy), udelhoven@uni-trier.de (T. Udelhoven), patrick.hostert@geo.hu-berlin.de (P. Hostert), hermann.kaufmann@gfz-potsdam.de (H. Kaufmann).

http://dx.doi.org/10.1016/j.rse.2015.04.001
0034-4257/

Stevens et al., 2008, 2010; Viscarra-Rossel, Walvoort, McBratney, Janik, & Skjemstad, 2006). However, the VNIR-SWIR can reach its limits on semi-arid soils due to their special spectral characteristics. Sandy soils (coarse textured) are common among semi-arid areas and their grain size distribution is crucially driven by the dominant mineral, quartz (SiO_2), which lacks any distinctive Si–O bond related spectral features within the VNIR-SWIR (Hunt & Salisbury, 1970). Quartz is the main mineral constituent of most soils on Earth. Furthermore, these soil particles are often coated with iron-oxides and/or -oxyhydroxides (hematite and goethite), which reveal a strong spectral contrast in the VNIR (Hunt, Salisbury, & Lenhoff, 1971) and thus, generally obscure any other potential spectral features in this spectral region, such as from soil organics (Ben-Dor, Inbar, & Chen, 1997). Other specific spectral features of semi-arid soils may occur from sparse vegetation and salts (Mougenot, Pouget, & Epema, 1993), or from cyanobacteria coatings (Karnieli, Kidron, Glaesser, & Ben-Dor, 1999).

In this context the thermal infrared (TIR) wavelength region within the atmospheric window between 8 and 14 μm (longwave infrared) shows good remote sensing potential to extend the scope of the VNIR-SWIR. Longwave infrared (LWIR) remote sensing depends on emitted radiance and the energy source is the object itself. Within the LWIR the strong fundamental molecular vibrations of the Si–O stretching produces reststrahlen bands with intense spectral contrast (Salisbury & D'Aria, 1992a). Diagnostic spectral features of typical clay minerals of soils (e.g. kaolinite, illite, and montmorillonite) are offered within the LWIR. The results from several studies have already indicated the prospects of the LWIR in geological studies (Cudahy et al., 1999, 2012; Cudahy, Whitbourn, Connor, Mason, & Phillips, 1999; Hecker, van der Meijde, & van der Meer, 2010; Hecker, Dilles, van der Meijde, & van der Meer, 2012; Hewson, Cudahy, Mizuhiko, Ueda, & Mauger, 2005; Ninomiya, Fu, & Cudahy, 2005; Notesco et al., 2014; Rowan & Mars, 2003; Whitbourn et al., 1997; Yitagesu, van der Meer, van der Werff, & Hecker, 2011) and for vegetation investigations (Elvidge, 1988; Ribeiro da Luz & Crowley, 2007; Schlerf et al., 2012; Ullah, Schlerf, Skidmore, & Hecker, 2012).

Previous soil science studies that utilize LWIR spectroscopy to quantify soil properties predominantly use Diffuse Reflectance Infrared Fourier Transform (DRIFT) Spectroscopy (Janik, Merry, & Skjemstad, 1998; McCarty, Reeves, Reeves, Follett, & Kimble, 2002). However, DRIFT Spectroscopy does not comply with the requirements necessary for a quantitative comparison with emission spectra obtained via thermal infrared remote sensing (Salisbury & D'Aria, 1992a; Salisbury, Walter, Vergo, & D'Aria, 1991) as such measurements do not adequately account for radiation scattered in all directions (Nerry, Labed, & Stoll, 1990; Salisbury, Wald, & D'Aria, 1994; Sobrino et al., 2009). Directional Hemispherical Reflectance (DHR) as an active spectroscopic method or emission spectroscopy (passive mode) in combination with temperature emissivity separation (TES) algorithms was found to be adequate to accurately recover emissivity (Hecker et al., 2011).

Sobrino et al. (2009) demonstrated that DHR measurements of soils exhibit spectral features of crucial soil minerals in the LWIR. From ASTER-LWIR imagery data, soil properties (e.g. sand content) and soil mineral composition (e.g. abundance of calcite, mica, smectite, kaolinite) were successfully quantitatively derived by Breunig, Galvao, and Formaggio (2009, 2008); Breunig, Galvao, Formaggio, and Couto (2009) and Mulder, de Bruin, Weyermann, Kokaly, and Schaepman (2013). Sobrino, Franch, Mattar, Jiménez-Muñoz, and Corbari (2012) also estimated soil moisture from the LWIR via ASTER and AHS (Airborne Hyperspectral Scanner) imagery data.

The aim of this study is to evaluate the potential of the LWIR wavelength range for quantitative mapping of soil properties — especially for semi-arid agricultural areas dealing with coarse textured soils. Our laboratory-based analyses not only apply to the laboratory-scale, but provide an important background for airborne and ultimately also for future spaceborne monitoring concepts, as we simulated the spectral resolution of air- and space-borne sensors. All parameters have been chosen so they are still representative for remote sensing studies as well. Measurements were collected with emission spectroscopy in the 8–14 μm LWIR atmospheric window as a proxy for air- and spaceborne data. The purpose of this study was to investigate if these LWIR spectral bands could overcome the limitations of the VNIR-SWIR for quantifying soil properties and have the capabilities to detect and quantify small ranges of the soil properties sand-, clay, and SOC content, as they appear in the semi-arid agricultural landscapes of Mullewa in Western Australia, at laboratory and remote sensing spectral resolution.

Preliminary findings of this study were published in Eisele et al. (2012) focusing on the prediction of sand, clay, and SOC content at laboratory scale from VNIR-SWIR and LWIR spectroscopy. We present in this paper new research aiming at (1) a deeper understanding of the interactions between the soil samples and their LWIR spectral signatures through the use of different LWIR emission measurement techniques and a more accurate characterization of the soil properties based on mineralogical and geochemical analyses, and (2) we also present new results on the predictions of the soil properties (sand-, clay, and SOC content) and the soils' geochemical properties (SiO_2 and Al_2O_3 content) using spectrally-degraded VNIR-SWIR and LWIR data that simulate airborne (HyMap, TASI) and satellite (ASTER) conditions. In particular, a more profound interpretation of the LWIR spectral signature is presented, based on the consideration of new and improved LWIR emission measurements (obtained via a MIDAC spectrometer) and a different TES algorithm, which led to more accurate emissivity signatures. Also, we focused the predictions of the soil texture properties (sand and clay content) in this study on the predominant agricultural samples sites, with more homogeneous texture characteristics in order to have a more robust spectral modeling focused on coarse-texture soils.

2. Materials and methods

2.1. Investigation area, soil sampling, and sample analyses

The soil samples investigated in this study originated from the marginal edges of the Western Australian wheatbelt region. The semi-arid area is located west of the township Mullewa (28°32′15″S, 115°30′25″E) and is a test site of the Department of Agriculture and Food of Western Australia (DAFWA), as the vulnerability of these soils to wind erosion is regarded as to high and very high (Rogers, 1996). Thus, farmers in this region mainly practice a conservation tillage system. The area is dominated by an undulating sand plain system, which includes yellow and red sands. An alluvial valley system includes relict red loams over red-brown hardpans, respectively classified as Tenosols and Kandosols, in the Australian Soil Classification (Isbell, 1996).

The soil sampling was carried out under dry conditions in accordance with an airborne flight campaign in February 2010. Nine flight lines have been recorded from two sectors (west and east) via the hyperspectral Sensor HyMap as shown in Fig. 1. From both sectors circular sample plots with a diameter of 15 m have been selected within the agricultural cropland (paddocks) and in the vicinity around the paddocks. Within these circular areas soil was scraped randomly from the upper soil horizon (<20 mm depth) to fill a 500-gram sample bag. 137 soil samples were taken and subsequently air-dried and passed through a 1 mm sieve.

From all 137 soil samples the mineralogy and geo-chemistry were determined from X-ray diffraction (XRD) and X-ray fluorescence (XRF) analyses. A few of the non-agricultural soil samples were classified as alkaline clays (Vertisols). These soils had much higher clay contents (~60%) than the samples collected in the paddocks, and thus stretched the range of soil characteristics of the dataset, which was used in the quantification of the soils' geochemical properties (SiO_2 and Al_2O_3 content).

For the analysis of the soil properties (sand, clay, and SOC content) only the soil samples from the western sector were available (Fig. 1). The grain size distribution was determined through sieving and sedimentation using the pipette method (McKenzie, Henderson, &

Please cite this article as: Eisele, A., et al., Advantages using the thermal infrared (TIR) to detect and quantify semi-arid soil properties, *Remote Sensing of Environment* (2015), http://dx.doi.org/10.1016/j.rse.2015.04.001

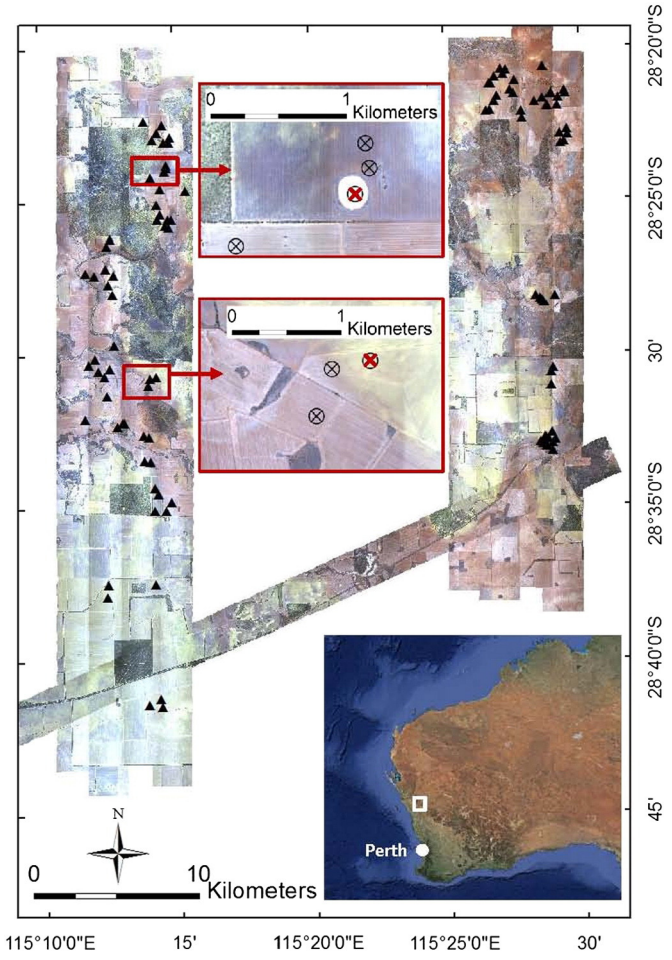

Fig. 1. Investigated area in the Western Australian wheatbelt region (~500 km north of Perth). The triangles mark the locations where surface soil samples have been taken within circular plots with a diameter of 15 m (circles are not scaled). Red-crossed are two sample plots where LWIR spectral measurements have been taken in the field from the soil surfaces with an emission FTIR spectrometer.

McDonald, 2002) to obtain clay (<2 μm), silt (2–20 μm), and subsumed sand (20–1,000 μm) size fractions. The soils' organic components have been removed with hydrogen peroxide before the grain size distribution analyses. Soil organic carbon (SOC) content was measured using the Walkley–Black method (Walkley & Black, 1934). 53 of the soil samples in sector west were taken within paddocks and were used for the prediction of the SOC content. These 53 agricultural samples predominantly showed a small range in texture (<15% clay and >85% sand content) with only a few clay rich samples (~30% clay content). Incorporating such non-typical, clay rich samples, and thus modeling the soils' clay and sand content across this data gap is feasible (Eisele et al., 2012) but would result in too optimistic prediction models with a very high predictive accuracy (R^2). For a constant predictive precision an increasing range of the response variable (e.g. clay content) would result in unjustified increasing R^2-values in the partial least squares regressions, as shown in Eisele (2014). The focus of this research is to map textural changes of coarse textured soils as accurate as possible, as they are more likely affected by wind erosion. We used 41 samples for the quantification of the soils' clay and sand content, which covered the dominating textural range < 15% clay and >85% sand content to support the aim of this paper and enable a profound spectral interpretation based on robust prediction models. This textural range is representative for a typical distribution on the paddocks in the marginal edges of the Western Australian wheat belt region as can be seen in Kobayashi et al. (2010). They independently sampled paddocks within the same area and obtained a similar textural distribution with sandy soils as the dominant composition.

The datasets used for the quantitative analyses of this study are described in Table 1. Only the clay and the sand contents have been used as soil texture properties in this study. The complementary silt fraction was not considered. In this study clay or sand content refers to the clay or sand fraction determined in the grain size distribution analyses, and the soils' grain size (or particle size) distribution is referred to as the soils' texture.

2.2. Soil spectroscopic measurements

2.2.1. LWIR emission spectroscopy

The soils' spectral signatures in the LWIR were acquired via emission FTIR spectroscopy, a passive emission mode method, measuring the radiance emitted by the sample itself. The spectra were recorded at ITC (*Faculty of Geo-Information Science and Earth Observation of the University of Twente*) spectral laboratory in Enschede using a portable MIDAC spectrometer (Model Illuminator M4401 — http://midac.com/illuminator.html) equipped with customized foreoptics. The foreoptics contain a flat folding mirror on a rotational axis that allowed the viewing of the sample or one of the two calibration blackbodies built into the foreoptics. The MIDAC used a liquid-nitrogen-cooled Mercury Cadmium Telluride (MCT) detector and recorded interferograms with a spectral resolution of 4 cm^{-1} (~40 nm @ 10 μm; sampling interval ~ 3.86 cm^{-1}) within the spectral range from 2.5 to 20 μm. However, for this study the spectral range was reduced to 7–14 μm, due to decreasing signal strength outside this range. The instrument's field of view (using a cut-off of 5% of the maximum responsivity) has a starting diameter of 53 mm at the folding mirror and spreads with about 18 mrad. For this measurement series, the samples and an Infragold plate were placed 100 mm below the folding mirror, resulting in a sampling spot with a diameter of 55 mm.

The radiometric calibration of the instrument and the downwelling radiance measurement are not described in full length here, but can be found in Eisele et al. (2012), which adopted methods of Hook and Kahle (1996) and Salisbury et al. (1994) for a similar emission FTIR instrument (Design and Prototypes μFTIR-102). The temperature emissivity separation method (BBfit), applied to calculate emissivity values, is described in detail by Salvaggio and Miller (2001).

2.2.1.1. Radiometric calibration and downwelling radiance measurements. The instrument was radiometrically calibrated before each sample by using radiance measurements from two individual blackbodies, set to 70 °C (BB_{hot}) and 20 °C (BB_{cold}). Gains and offsets were calculated from these readings assuming a linear relationship between the instrument's raw digital number (DN) values and the calculated at sensor radiance. Downwelling radiance (DWR) was measured, to derive the quantitative influence of the laboratory background self-emission (e.g. walls, celling, etc.), which was included within the sample measurements. A highly diffuse reflecting gold plate (Infragold®) with an emissivity (ε) of ~0.05 was used to collect DWR, right after the two blackbody measurements and just before the sample reading. The laboratory background temperature and the temperature of the gold plate were assumed to be equal due to sufficient time of acclimatization.

Table 1
Descriptive statistics of the soil properties (sand, clay, and soil organic carbon (SOC) content) and the soils' geo-chemistry (SiO_2 and Al_2O_3 content) based on laboratory analyses (number of samples (n), mean, standard deviation (SD), maximum (Max), minimum (Min), median, 25% percentile (Q1), and 75% percentile (Q3)).

	n	Mean	SD	Max	Min	Median	Q1	Q3
SAND (%)	41	92.01	2.33	95.30	85.50	92.20	91.20	93.30
CLAY (%)	41	6.62	2.03	12.60	3.80	6.80	4.90	7.60
SOC (%)	53	0.51	0.22	1.12	0.17	0.46	0.34	0.60
SiO_2 (%)	137	89.59	6.26	97.00	60.30	91.60	87.40	93.60
Al_2O_3 (%)	137	4.50	2.58	14.80	0.90	3.70	2.60	6.00

2.2.1.2. Soil sample radiance measurements. The soil samples were heated in a forced-air oven to 70 °C for a minimum of 4 h. This allowed the samples to be much hotter in relation to the background room temperature during the measurement, which ensured an improved signal-to-noise ratio (SNR). The samples were measured straight after being removed from the oven and 64 scans were integrated (resulting in a measurement time of about 15 s) to keep the decrease in temperature to a minimum while recording the spectra.

2.2.1.3. Temperature emissivity separation (TES). The retrieval of the soil surface emissivity requires the knowledge of the exact surface temperature at the time of measurement. This is estimated using an inverse Planck curve fitting algorithm (BBfit), called temperature-emissivity separation (TES), which we applied to the spectral region between 7 and 7.5 μm. We assumed this range to be close to ε ~ 1.0 due to the predominance of the quartz-rich mineralogy among the Mullewa soil samples and thus, the associated Christiansen frequency feature of quartz within this wavelength region.

2.2.2. DHR FTIR spectroscopy

To assess the accuracy of the LWIR emission spectroscopy approach, we measured a reference material consisting of sand sized particles of quartz (grain size: 200–800 μm; 99.95% SiO_2 content) for its directional–hemispherical reflectance (DHR). In contrast to passive mode emission FTIR spectroscopy, active mode DHR spectroscopy does not depend on a controlled and stabilized sample temperature and is not influenced by downwelling radiance. A Perkin&Elmer FTIR spectrometer (model: Spectrum GX) with an external integrating sphere (100 mm diameter, 25 mm sample port in a down-looking mode) was used for the DHR measurements at GFZ (*German Research Centre for Geosciences in Potsdam*). The spectra were recorded with a spectral resolution of 4 cm^{-1}. To improve the SNR we integrated 2048 scans for the quartz sand and 256 scans for the background measurements, which took approximately 40 min per sample. A comprehensive discussion about the DHR FTIR spectroscopy can be found in Hecker et al. (2011).

2.2.3. VNIR-SWIR diffuse reflectance spectroscopy

Soil surface bidirectional reflectance in the VNIR-SWIR spectral region was measured in the laboratory using an Analytical Spectral Devices (ASD) Inc. FieldSpec-Pro Full Range (http://www.asdi.com) spectrometer. Soil samples were illuminated with a 1000 W quartz-halogen lamp with a zenith angle of 30°. The reflected light was collected from a nadir position using a bare-fiber (23° field of view, FOV) at a height of 100 mm. This resulted in a sampling spot size of ~50 mm, making it comparable with that of the MIDAC system. The spectral resolution of the ASD was 3–4 nm in the 0.35- to 1.0-μm region (spectral sampling 1.4 nm), and 10–12 nm in the 1.0- to 2.5-μm region (spectral sampling 2 nm). The entire spectrum was resampled at 1 nm for display purposes, which resulted in 2151 spectral bands. The ASD spectra were subsequently corrected to relative reflectance using the white reference measurement of a Spectralon® panel (http://www.labsphere.com) as a reference.

2.3. Spectral processing

To closely meet the spectral requirements of a remote sensing approach, we reduced the spectral range of the spectral signatures in accordance with atmospheric windows, where electromagnetic radiation is allowed to pass without significant attenuation. Within the atmospheric windows we defined a spectral range, which was available with the study's spectrometers and not considered to be significantly influenced by noise. For the multivariate data analyses we used the LWIR spectra from 7.9 μm to 12.3 μm, which resulted in 118 bands for full spectral resolution of the MIDAC spectrometer. The VNIR-SWIR spectra were used in the wavelength region from 0.4 μm to 2.45 μm, with the exclusion of potential water vapor bands between 1.35 and 1.45 μm and between 1.85 and 2.05 μm. This leads to 1753 ASD bands. To be consistent with the Beer–Lambert's law (Esbensen, 2006), the LWIR and the VNIR-SWIR soil spectra were transformed from reflectance (R) to absorbance ($\log_{10}(1/R)$) and used as input for the multivariate data analyses.

The soil signatures were used in full spectral resolution as measured with the particular spectrometer, and in addition, were spectrally resampled to multi- and hyperspectral sensor specifications. For the VNIR-SWIR the spectral response functions (SRF) of the airborne hyperspectral HyMap sensor (HyVista, http://www.hyvista.com) and the multispectral ASTER sensor, on board the Terra space platform (http://asterweb.jpl.nasa.gov), were used to simulate the soils' spectral responses. The LWIR spectra were resampled to the SRF characteristics of the hyperspectral airborne sensor TASI-600 (ITRES, http://www.itres.com) and to the multispectral LWIR sensor of ASTER. The sensors' specifications are summarized in Table 2. Nine out of 125 HyMap bands have been excluded for this simulation due to their proximity to significant atmospheric water-absorption regions near 1.4 μm (4 bands) and 1.9 μm (5 bands), which resulted in 116 bands.

2.4. Multivariate data analyses

Partial least squares (PLS) regression (Wold, Sjöström, & Eriksson, 2001) — applying the NIPALS algorithm (Martens & Naes, 1992) — was used to model and predict the soil properties from the soil spectral signatures. PLS regression is a well-established quantification technique and is tailored especially to spectroscopic requirements: overlapping spectral response functions (multicollinearity), more spectral bands than measured samples, and instrument noise. Furthermore, PLS offers the option to interpret the prediction models in terms of their relevant spectral influences via the regression coefficients and/or the loading weights (Esbensen, 2006).

The performance of a PLS-model was assessed by employing a full cross-validation ("leave one out"). The following performance indicators were calculated for each PLS-model. The performance indicator for the predictive accuracy was the coefficient of determination (R^2), and for the predictive precision, the root mean square error of cross validation (RMSECV), the standard error of cross validation (SECV), and the systematic error (BIAS). Note, if the RMSECV and the SECV are similar, the BIAS is insignificant (Esbensen, 2006). As an accuracy index for the prediction models the RPD (Ratio of Performance to Deviation) was computed as the ratio of the standard deviation in the corresponding data set to the SECV. Three classes of RPD can be defined (Chang,

Table 2
Spectral characteristics of airborne and spaceborne sensors used in the spectral resampling.

	LWIR		VNIR-SWIR	
Sensor	TASI-600	ASTER	HyMap	ASTER
Spectral range	8.0–11.4 μm	8.3–11.3 μm	0.45–2.48 μm	0.52–2.43 μm
Number of bands	32	5	125	9
Spectral resolution (FWHM)	125 nm	350 nm (B10–B12) 700 nm (B13 & B14)	15–20 nm	40–100 nm

Please cite this article as: Eisele, A., et al., Advantages using the thermal infrared (TIR) to detect and quantify semi-arid soil properties, *Remote Sensing of Environment* (2015), http://dx.doi.org/10.1016/j.rse.2015.04.001

Laird, Mausbach, & Hurburgh, 2001): category A (RPD > 2) are models with accurate prediction abilities, category B (RPD between 1.4 and 2) is an intermediate class with models that can possibly be improved, and category C models (RPD < 1.4) with no prediction capability.

3. Results

To evaluate the emissivity signatures, which were derived from passive mode LWIR emission spectroscopy in terms of radiometric calibration, downwelling radiance measurement, and the TES method, we compared these spectra with the spectra derived from the active mode DHR measurement. Reflectance (R) of the DHR spectrum was brought to emissivity (ε) according to Kirchhoff's law, $\varepsilon = 1 - R$ (Nicodemus, 1965). The comparison is based on the quartz reference sand, which allows the assumption of a nearly analog surface for both measurements. Fig. 2 depicts these spectral signatures in the range between 7 and 14 μm. The comparison shows great consistency between the two quartz reference sand spectra and emphasizes that the emissivity values derived from the LWIR emission spectroscopy are appropriate for this study. The slight tilt effect, which can be diagnosed from 10 μm to longer wavelengths, could not be addressed. Note, that the cooling of the sample during the integration time of the measurement was not considered as a possible cause for this effect (Eisele, 2014).

The assumption we made in the TES ($\varepsilon \sim 1.0$ between 7 and 7.5 μm) proved to be a good choice for fitting the Planck curve, as for the quartz-dominated soils this region offered reliable constant high emissivity values. This can be seen from Fig. 2, which shows emissivity values close to $\varepsilon \sim 1.0$ within the defined spectral range with no noticeable discrepancy between the passive (TES applied) and the active (no TES needed) spectroscopic measurements. Strictly, for soils this assumption removes from its validity with decreasing sand content or SiO_2 content. However, even for the soil sample with the lowest sand and SiO_2 content in the investigated area (Cal9: 18.7% and 57.1%, respectively), the deviation was below 2% and was considered as negligible.

3.1. Soil spectral characteristics in the LWIR and in the VNIR-SWIR

The spectral signatures of 4 soil samples, which are representative of the investigation area, are displayed in Fig. 3 for the LWIR (A) and for the VNIR-SWIR (B). The figure additionally shows the spectrum of the quartz reference sand (black-dashed curve), which is the investigated soils' main mineral constituent. Note that sample Cal9 was found by textural analysis to have the highest clay content (68.4%) within the investigation area. This sample was taken away from the agricultural paddocks and thus was not considered in the predictions of the soil properties.

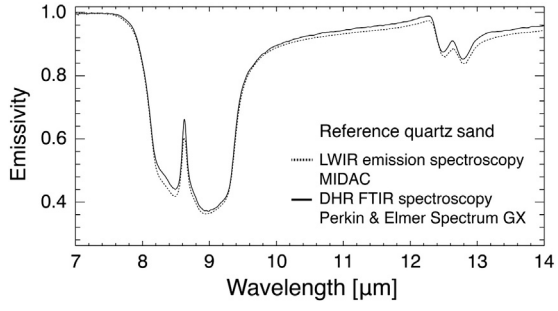

Fig. 2. Comparison of the spectral signatures of the reference quartz sand (99.95% SiO2 content) derived from the active mode reflectance directional hemispherical measurement (DHR-FTIR spectroscopy) and from the passive mode emission measurement (LWIR emission spectroscopy).

3.1.1. Spectral characteristics of quartz based mineralogy and the influence of iron

The LWIR soil signatures in Fig. 3-A demonstrate the characteristic spectral properties of quartz: the reststrahlen bands (RB) with its intense spectral contrast, which is produced by the strong fundamental molecular vibrations of the Si–O stretching. The RB are bordered on both sides by a Christiansen frequency feature (CFF) at 7.5 and at 12.3 μm, where the scattering is minimum, penetration into the material and thus emissivity (ε) is maximum (Salisbury, Hapke, & Eastes, 1987). Within the RB the distinct quartz doublet is apparent with an emissivity maximum at 8.6 μm.

The similarity in the mineralogy/texture of the quartz reference sand and the extremes among the coarse textured soil samples, such as Mu18 (94% sand and 5% clay content; 97% SiO_2 content), suggests similar spectral characteristics. But in the VNIR-SWIR (Fig. 3-B) the mismatch is obvious and can be largely attributed to the grain coating effects of iron-oxides (hematite) and -oxyhydroxides (goethite), which dominate the spectral soil signatures in the VNIR. Both of these iron bearing minerals show a strong spectral contrast until ~1.3 μm and their characteristic spectral features (Hunt et al., 1971; Viscarra-Rossel & Behrens, 2010) were evident among all measured soil spectra. However, the results of XRD analyses detected hardly any hematite and goethite, as these minerals occurred as thin, nano-crystalline layers with almost no grain volume. These thin mineral layers cease to exist in the powdered sample volumes by the grinding of the soil samples to a grain size < 20 μm for the mineralogical analyses. The quartz reference sand does not show any unique spectral characteristics throughout the VNIR-SWIR wavelength region.

3.1.2. Spectral features of clay minerals

In general, the LWIR can contain spectral information of several typical clay minerals of soils, such as kaolinite, illite and montmorillonite. This can be seen from the reference spectra of these minerals in Fig. 4, which are taken from the ASTER spectral library (Baldridge, Hook, Grove, & Rivera, 2009) and were converted to emissivity assuming Kirchhoff's law. Note that these reference spectra were measured in bi-directional (biconical) reflectance, which is a limitation in quantitative comparisons to emission measurements from remote sensing. In the spectral signatures of the soils samples from the paddocks in Mullewa the spectral features of kaolinite are evident at 9.0 μm, at 9.8 μm, at 10.5 μm, and at 10.95 μm (Fig. 3-A and A1). An additional lobe within the quartz doublet (i.e. a triplet) appears with the presence of kaolinite. Kaolinite was also identified in the XRD analyses as the dominating clay mineral among these soils. Moreover, the distinctive kaolinite doublet in the SWIR around 2.2 μm (2.16/2.209 μm) related to Al–OH-content (Hunt & Salisbury, 1970) emphasizes this mineralogy. Note that the spectral features in the VNIR-SWIR around 1.4 μm and 1.9 μm are related to H_2O/OH and H_2O, respectively, and are not available for remote sensing datasets due to atmospheric absorption.

3.1.3. Soil texture related spectral characteristics

In the LWIR the soil spectral signatures reveal diagnostic soil textural-related information. The LWIR spectra respond in accordance with the theory (Salisbury & D'Aria, 1992b) and display the characteristic reduction of the spectral contrast within the RB with increasing influence of smaller particles (Fig. 3-A).

For the VNIR-SWIR the general theory states that the overall reflectance increases with decreasing particle size, while the spectral contrast of the clay feature decreases (Baumgardner, Silva, Biehl, & Stoner, 1985; Ben-Dor, Irons, & Epema, 1999; Hunt, 1980). This was inconsistent with the spectral signatures of the investigated soils. However, an inverse trend can be recognized in the SWIR, which can be linked to the opaque part of the theory from Irons, Weismiller, and Petersen (1989), who further differentiates between opaque and transparent minerals (opaque minerals, including oxides, accordingly show inverse relationship to transparent minerals, which includes quartz). Even so, no robust

Please cite this article as: Eisele, A., et al., Advantages using the thermal infrared (TIR) to detect and quantify semi-arid soil properties, *Remote Sensing of Environment* (2015), http://dx.doi.org/10.1016/j.rse.2015.04.001

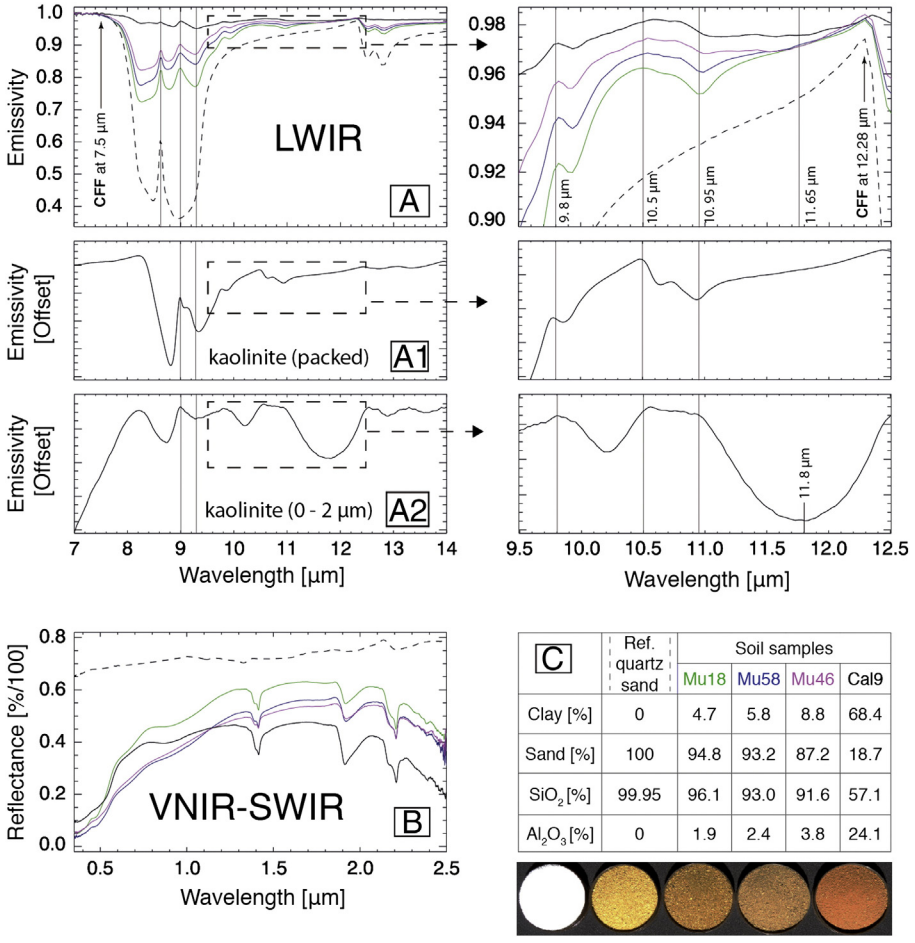

Fig. 3. Spectral signatures of soil samples (solid curves) from the Mullewa investigation area and from a reference quartz sand (dotted curves) in the LWIR (A) and in the VNIR-SWIR (B). The table (C) depicts the corresponding soil properties (clay and sand content) as well as the soils' geo-chemical properties (SiO_2 and Al_2O_3 content). For the LWIR the reference spectral signatures from the ASTER spectral library (Baldridge et al., 2009) of pure kaolinite are displayed in packed (A1), and in powder (A2) condition. On the right side of the LWIR plots the spectral ranges between 9.5 µm and 12.5 µm are displayed in more detail. Here fine-sized particles can cause volume scattering.

regularity related to the particle size could be observed for the overall reflectance of the soil spectra in the VNIR-SWIR. The reason was mainly seen in the influence of grain coatings, and thus conflicting particle size related behaviors. Although the continuum-removed absorption depth (CRAD) of the clay mineral spectral feature at 2.2 µm showed the potential to quantify the clay content in previous studies (Nanni & Demattê, 2006; Rodger & Cudahy, 2009), the small textural range of the sandy soils of Mullewa does not allow such a mono-causal approach (Fig. 5).

3.1.4. The influence of volume scattering on the soils' spectral signatures

The LWIR soil spectra showed additional texture-related spectral features between 9.5 and 12.5 µm (Fig. 3-A). For particulate materials the scattering processes in this spectral region are strongly influenced by the materials' particle sizes (Salisbury & Wald, 1992). While the LWIR is in large part controlled by surface scattering processes (exceptions are the CFFs), in the interaction between wavelength of 9.5–12.5 µm and very fine material (0–75 µm) the influence of the volume scattering becomes perceptible. This is demonstrated in Fig. 3-A2 in accordance with a reference spectrum of kaolinite powder (particle sizes: 0–2 µm). Here the volume scattering causes an emissivity trough with a minimum at 11.8 µm, a so called Transparency Feature (TF) (Salisbury & Walter, 1989).

This reference powder sample contains only clay-sized particles (100% clay content), whereas even the most clay-rich agricultural soil

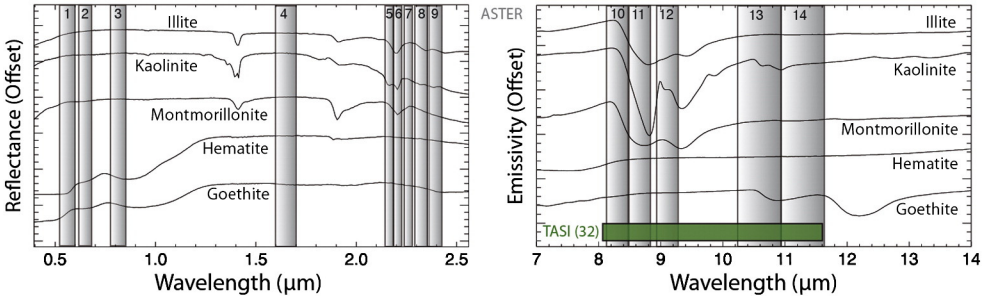

Fig. 4. Spectral signatures of typical semi-arid soil minerals from the USGS (Clark et al., 2007) and ASTER spectral library (Baldridge et al., 2009). The spectral bands of the spaceborne (ASTER-VNIR-SWIR, 9 bands and ASTER-LWIR, 5 bands) and airborne (TASI, 32 bands) sensors used in the spectral resampling are highlighted in gray and green, respectively.

Please cite this article as: Eisele, A., et al., Advantages using the thermal infrared (TIR) to detect and quantify semi-arid soil properties, *Remote Sensing of Environment* (2015), http://dx.doi.org/10.1016/j.rse.2015.04.001

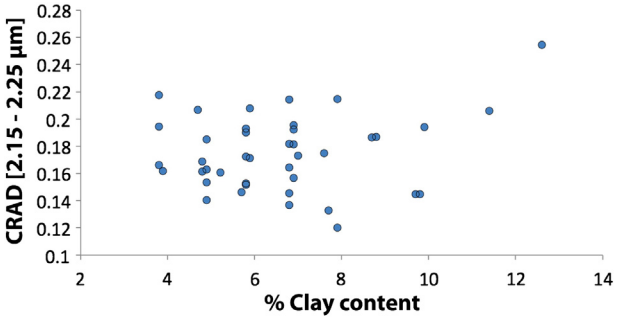

Fig. 5. Clay content of the soil texture data set (41 samples) versus the continuum-removed absorption depth (CRAD) of the VNIR-SWIR spectra between 2.15 µm and 2.25 µm.

samples taken for the prediction have less than 15% clay content with a mean value of approximately 7%. However, even these coarse textured soils reveal the influence of the volume scattering. This is already noticeable for lower clay contents, as the influence of the TF modifies other spectral features in this region. This can be observed from the kaolinite feature at 10.95 µm, which is apparent as a distinct emissivity minimum in the coarse textured samples (e.g. Mu18: 4.7% clay content) and gets successively reduced with increasing clay content. For the soil samples with comparably high clay content (e.g. Mu46: 8.8% clay content) the LWIR signature clearly indicates the built up of the TF.

3.1.5. Minerals in the soils' grain coatings

The distinct emissivity minimum at 10.95 µm coincides with the same feature of the reference spectrum of packed kaolinite powder (Fig. 3-A1), which simulates the spectral character of coarse textured surfaces (Wald & Salisbury, 1995). Thus, we assume that the distinct emissivity minimum at the 10.95 µm is caused by surface scattering from kaolinite within the soils' grain coatings. This conclusion is supported by the fact that these extremely sandy soils, such as Mu18, showed very little clay-sized particles in the grain size distribution analyses. However, the spectral features for kaolinite were strong and distinct for these coarse textured soils in both the LWIR (9.0, 9.8, 10.5, and 10.95 µm) and the SWIR (2.16/2.209 µm). Hence, in addition to the hematite/goethite grain coatings, we assume that these soils also exhibit kaolinite within their grain coatings. This was also observed by Lyon (1990), who interpreted similar VNIR-SWIR signatures of coarse textured Western Australian soils, as caused by iron-oxides and aluminosilicates within the grains' "desert varnish coatings".

While the iron-bearing minerals within the grain coatings were spectrally evident only in the VNIR-SWIR (the thermal infrared wavelength did not have enough energy to trigger the necessary electron charge transfer processes, and thus these iron bearing coatings were transparent for the LWIR), the kaolinite within the grain coatings was evident in the soil spectra of both wavelength regions, in the VNIR-SWIR and in the LWIR.

3.2. Prediction of soil properties (sand, clay, and SOC content)

PLS-calibration and -validation were realized with the LWIR and the VNIR-SWIR spectral signatures for the soil properties sand-, clay-, and SOC content. The descriptive statistics of the datasets that were used are summarized in Table 1, and the PLS-models' performance indicators for the validation stage are summarized in Tables 3, 4, and 5. The models' y-variances are displayed in Fig. 6.

3.2.1. Full spectral resolution

3.2.1.1. Soil texture properties (sand and clay content). Both soil texture properties (sand and clay content) could be predicted with high precision from the LWIR soil spectra with full spectral resolution ($RMSECV_{SAND}$: 0.986%; $RMSECV_{CLAY}$: 0.980%). Both models showed a high predictive accuracy, as they were able to explain a large part of the soil properties' variances (y-variance = $R^2 * 100$) (R^2_{SAND}: 0.826; R^2_{CLAY}: 0.772). Only 4 factors were needed to establish robust models for the sand and the clay content. For both properties the explained variances were close between calibration (blue) and validation (red) (Fig. 6-A1 and B1), thus, overfitting in these models was low. The robustness of these models was also demonstrated from the uniform development (quasi-parallel) of the explained variance between calibration and cross-validation over the number of model factors.

To determine the models' spectral drivers, their regression coefficients (RC) were interpreted (Fig. 7). The RC were calculated from the models' loading weights (calculated for each model factor), which represent a direct link between the spectral space and the corresponding predicted soil property (Esbensen, 2006). The models for predicting the sand and the clay content were both driven by the same spectral drivers (Fig. 7-A1 and B1), but were modeled inversely, as was expected from their high negative correlation. The RC of the soil texture models showed large influence at 9 µm and to a lesser degree at 9.8 µm. These wavelengths correspond to emissivity peaks of kaolinite. The peak in the corresponding RC at 9 µm (or 9.8 µm) indicates that this spectral feature is (1) important and (2) its importance drops from 9 µm (or 9.8 µm) in both directions.

Besides these mineralogical spectral drivers these models also presented soil texture related spectral drivers. On the one hand, this was evident as an ascent (sand content) / descent (clay content) towards the quartz doublet. This ascent is associated with the described theory of the grain size related reduction of the spectral contrast within the reststrahlen bands (driven by surface scattering). And on the other hand, this could be seen as a volume scattering induced particle size related modification for the spectral response at wavelengths less and greater than the 10.95 µm-feature (Note, that also these transition points (RC = 0) between increasing and decreasing influence marked wavelength which were important for the models.). Thus, the soil texture models could benefit from both mineralogical and particle size related spectral drivers.

Quantifying the soil texture properties from the VNIR-SWIR produced less stable models than from the LWIR, which was immediately

Table 3
PLS-model performance indicators for the soil spectral signatures in their full spectral resolution (number of samples (n), number of model factors used (f), coefficient of determination (R^2), root mean square error of cross validation (RMSECV), standard error of cross validation (SECV), systematic error (BIAS), and the ratio of performance to deviation (RPD)).

	n	LWIR (full-resolution)						VNIR-SWIR (full-resolution)					
		f	R^2	RMSECV	SECV	BIAS	RPD	f	R^2	RMSECV	SECV	BIAS	RPD
SAND	41	4	0.826	0.986	0.997	−0.037	2.34	7	0.566	1.557	1.579	0.055	1.48
CLAY	41	4	0.772	0.980	0.992	−0.002	2.05	7	0.537	1.398	1.413	−0.072	1.44
SOC	53	6	0.778	0.104	0.105	−0.004	2.10	4	0.571	0.144	0.146	−0.002	1.51
SiO_2	137	3	0.918	1.800	1.807	−0.004	3.46	9	0.784	2.919	2.931	0.049	2.14
Al_2O_3	137	3	0.911	0.772	0.775	−0.002	3.33	11	0.826	1.079	1.083	−0.02	2.38

Table 4
PLS-model performance indicators for the soil spectral signatures resampled to TASI (LWIR) and to HyMap (VNIR-SWIR).

	n	LWIR (resampling TASI)						VNIR-SWIR (resampling HyMap)					
		f	R^2	RMSECV	SECV	BIAS	RPD	f	R^2	RMSECV	SECV	BIAS	RPD
SAND	41	4	0.791	1.080	1.092	−0.035	2.13	7	0.513	1.649	1.670	0.019	1.40
CLAY	41	4	0.768	0.990	1.001	−0.004	2.03	7	0.520	1.423	1.440	−0.053	1.41
SOC	53	6	0.733	0.114	0.115	−0.004	1.91	4	0.608	0.138	0.139	−0.002	1.58
SiO_2	137	3	0.910	1.881	1.888	−0.015	3.32	9	0.776	2.972	2.984	0.031	2.10
Al_2O_3	137	3	0.908	0.786	0.789	−0.004	3.27	11	0.837	1.048	1.051	−0.008	2.45

evident from the development of their explained variances over the number of model factors (Fig. 6-D1 and E1). Both VNIR-SWIR models, for the sand and the clay content, showed large differences in the explained variances between model calibration and validation. This means that the texture properties were partially modeled (calibrated) from spectral information, which could not be found in the validation stage again. It can be assumed that noise (in the sense of information which is not related to the soil property) was a large factor in these models. Consequently, these models were predominately influenced by overfitting and would reveal their sensitivity in further predictions. Compared to the LWIR, the VNIR-SWIR models needed more factors (Sand: 7; Clay: 7), and with these they explained less of the y-variance (R^2_{Sand}: 0.566; R^2_{Clay}: 0.537) with less precision ($RMSECV_{Sand}$ 1.557%; $RMSECV_{Clay}$: 1.398%).

The spectral Interpretation from the RC (Fig. 7) was more difficult for the VNIR-SWIR models because of the large number of model factors (additional model factors comprise additional loading weights, which successively weakens the information of the inherent relationships within the final RC, comprising all loading weights). However, from the RC it was observed that in addition to the SWIR features (shown by the kaolinite doublet at 2.16/2.209 μm) the VNIR response had a large influence on the soil texture models (e.g. spectral features of hematite and goethite) (Fig. 7-A2 and B2). A deeper look inside the models via an interpretation of their loading weights (not shown here), confirmed the assumption that the VNIR-SWIR models predicted the sand and the clay content primarily via the spectral features of the soils' iron based grain coatings. As these spectral drivers — hematite and goethite — are not directly associated with the soils' grain size distribution, this resulted in comparable complex prediction models. In the discussion section we made one possible explanation to that effect.

3.2.1.2. Soil organic carbon (SOC). Both wavelength regions, the LWIR and the VNIR-SWIR, were dominated by mineralogical spectral influences. Nevertheless the content of soil organic carbon (SOC) could be predicted from the LWIR with good performance (R^2: 0.778; RMSECV: 0.104%), and also, to a lesser degree, from the VNIR-SWIR soil spectra (R^2: 0.571; RMSECV: 0.144%). But both models were mainly driven by indirect relationships and not by direct optical features of organic functional groups. This increased the models' complexity regarding the relationships between spectral features caused by vibrations of a specific functional group and the response variable.

The models' complexity can be seen for the LWIR from the additional model factors in Fig. 6-C1, which were needed to reach the maximum value of the explained y-variance and to guarantee at the same time minimum overfitting to obtain a preferable robust model for further predictions. The spectral interpretation of the SOC models from the RC was more difficult than of the soil texture models in the LWIR, due to additional model factors (Fig. 7-C1). The mineralogical influence, however, was evident from the RC, where the kaolinite spectral features at 9.0 μm and at 9.8 μm could be identified. Furthermore, the RC of the SOC model revealed two other major influences, which were associated as primarily quartz spectral features, diminished by the influence of increasing SOC content: (1) the wavelength position of the reflection point around 8.1 μm within the steep ascent from the CFF (at 7.5 μm) towards the first lobe of the quartz doublet, and (2) the descent towards the CFF at 12.3 μm. Noticeable influence could also be determined from the wavelength within the first lobe of the quartz doublet until 8.6 μm, which could also be the result of a diminished quartz feature (emissivity maximum at 8.6 μm), but is also in accordance with the wavelength region, where spectral active organic components such as carboxylic acids, aliphatic OH, polysaccharides, or cellulose have been found (Bornemann, Welp, & Amelung, 2008, 2010; Bornemann, Welp, Brodowski, Rodionov, & Amelung, 2008; Haberhauer, Rafferty, Strebl, & Gerzabeck, 1998; Rumpel, Janik, Skjemstad, & Kogel-Knabner, 2001; Solomon, Lehmann, Kinyangi, Liang, & Schafer, 2005).

In the VNIR-SWIR the SOC model reached its comparable low maximum in the y-variance (R^2: 0.571) after 4 factors and thus required fewer factors than the soil texture models, and also showed less overfitting in this region (Fig. 6-F1). The RC showed that the models were predominantly selecting the wavelength of the VNIR to predict the SOC content (Fig. 7-C2). This corresponds with the wavelength region where organic soil components have been found to be spectrally active (Ben-Dor & Banin, 1995; Ben-Dor et al., 1997). We attributed this influence to the spectral features of the iron-bearing grain coatings (hematite and/or goethite), which were evident in the model's loading weights of all four factors (Figs. 4 and 8). The SWIR, where spectral features of soil organic components also have been identified (Viscarra-Rossel & Behrens, 2010), showed minor influence in this prediction model.

3.2.2. Resampling to multi- and hyperspectral sensor specifications

The same LWIR and VNIR-SWIR soil spectral signatures were spectrally resampled to multi- and hyperspectral sensor specifications (VNIR-SWIR: HyMAP, $ASTER_{VNIR\text{-}SWIR}$; LWIR: TASI, $ASTER_{LWIR}$). Based on these resampled soil spectra PLS models were established for the same datasets and for the same soil properties (sand-, clay-, and SOC content). The PLS-models' performance indicators for the validation

Table 5
PLS-model performance indicators for the soil spectral signatures resampled to 5 ASTER-LWIR bands and to the 9 ASTER-VNIR-SWIR bands.

	n	LWIR (resampling to 5 ASTER bands)						VNIR-SWIR (resampling to 9 ASTER bands)					
		f	R^2	RMSECV	SECV	BIAS	RPD	f	R^2	RMSECV	SECV	BIAS	RPD
SAND	41	4	0.758	1.161	1.176	0.004	1.98	2	0.105	2.23	2.26	0.017	1.03
CLAY	41	4	0.728	1.072	1.085	−0.002	1.87	2	0.179	1.861	1.884	−0.021	1.08
SOC	53	5	0.383	0.173	0.175	0.001	1.26	3	0.579	0.143	0.144	−0.001	1.53
SiO_2	137	3	0.883	2.15	2.158	0.023	2.90	7	0.719	3.326	3.338	0.019	1.88
Al_2O_3	137	3	0.867	0.946	0.949	−0.007	2.72	7	0.694	1.433	1.438	−0.003	1.79

Please cite this article as: Eisele, A., et al., Advantages using the thermal infrared (TIR) to detect and quantify semi-arid soil properties, *Remote Sensing of Environment* (2015), http://dx.doi.org/10.1016/j.rse.2015.04.001

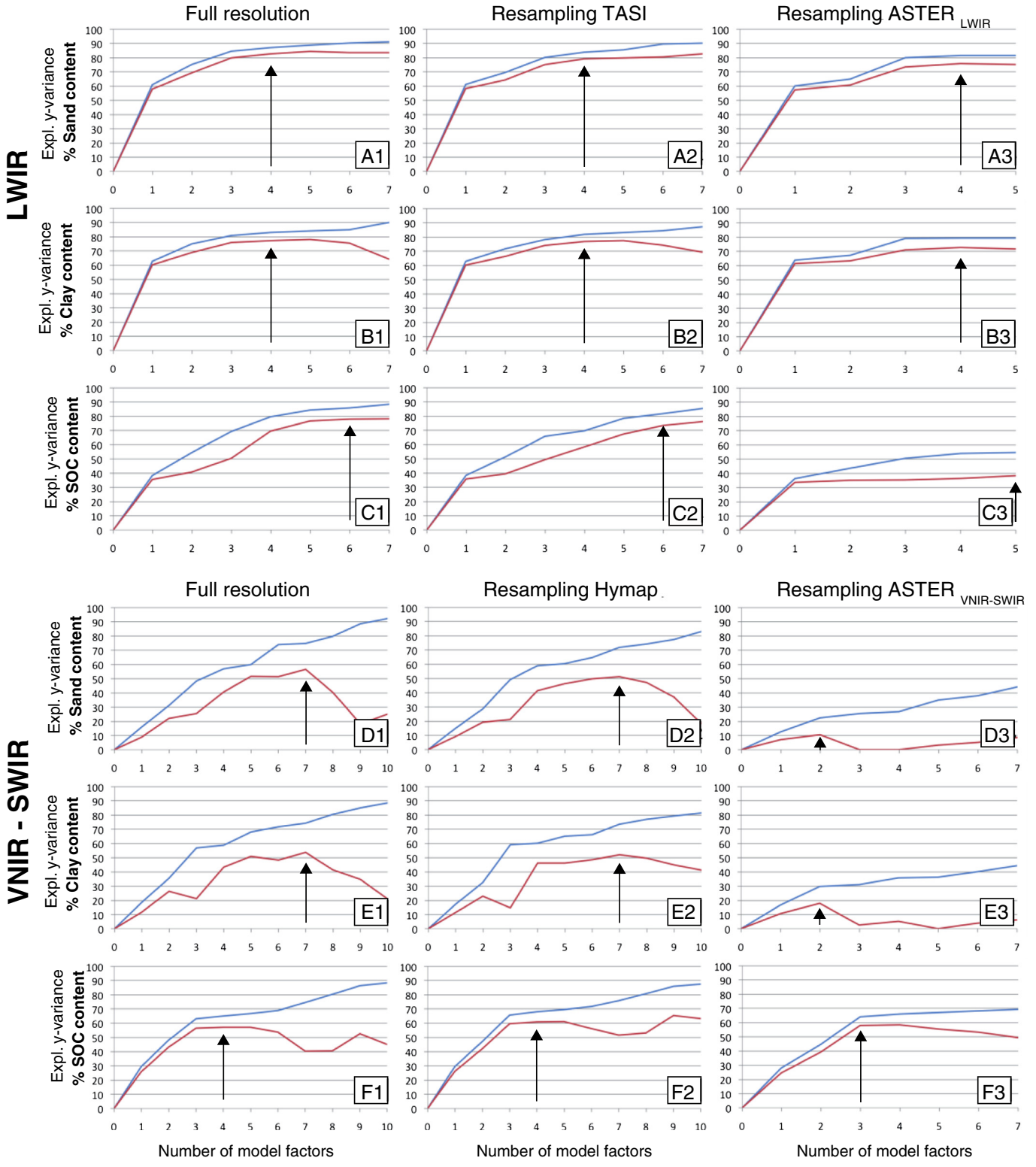

Fig. 6. Explained y-variance of the predicted parameters sand, clay, and SOC content in the PLS-models based on the LWIR (A, B, C) and the VNIR-SWIR (D, E, F) soil spectra in the full spectral resolution (1), and for the spectral resampling on TASI/HyMap (2), and $ASTER_{LWIR}$/$ASTER_{VNIR\text{-}SWIR}$ (3). Calibration indicates the blue and cross-validation the red curve. The arrows indicate the number of model factors used in the predictions. (For interpretation of the references to color in this figure legend, the reader is referred to the web version of this article.)

stage are summarized in Tables 4 and 5. The models' y-variances are displayed in Fig. 6.

The decreasing spectral dimensionality of the LWIR showed little influence on the performance indicators for the prediction models of the sand and clay content. Using the multispectral $ASTER_{LWIR}$-resolution (5 spectral bands) these soil texture properties could be predicted with only a slightly decreased accuracy (R^2_{Sand}: 0.758; R^2_{Clay}: 0.728) and precision ($RMSECV_{Sand}$: 1.161%; $RMSECV_{Clay}$: 1.072). However, the prediction of the SOC content using the multispectral $ASTER_{LWIR}$-resolution was degraded by this spectral band reduction (R^2_{SOC}: 0.383). The difference could be seen from the development of the y-variances in Fig. 6. The models of the texture properties (sand and clay

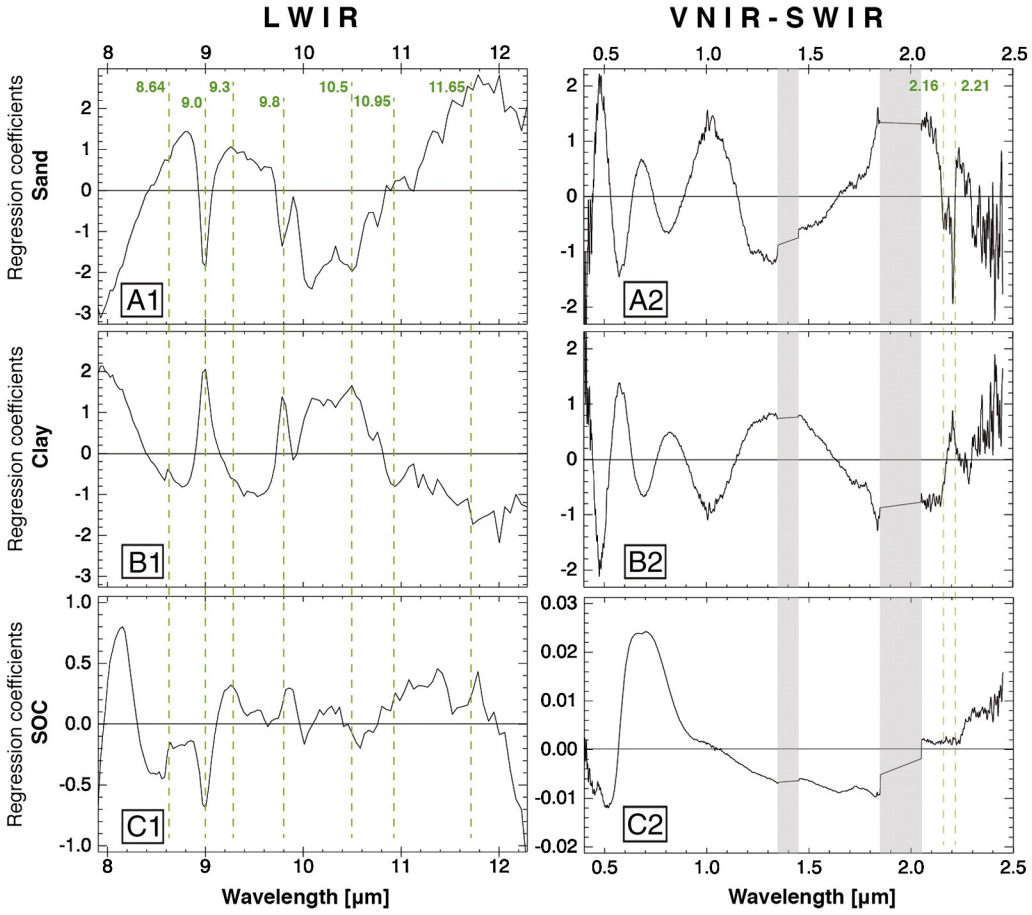

Fig. 7. Regression coefficients (RC) of the PLS-models (clay, sand, and SOC content) based on the LWIR and based on the VNIR-SWIR soil spectra (full spectral resolution). The dashed green lines indicate wavelength positions of spectral drivers which correspond to identified mineral spectral features (see Fig. 3). VNIR-SWIR-bands which have been ignored in the prediction models due to their proximity to significant atmospheric water-absorption are highlighted in gray.

content) were able to explain a large proportion of the y-variance on a constant level down to the multispectral $ASTER_{LWIR}$-resolution and remained very robust (Fig. 6-A1 to A3 and B1 to B3). The proportion of the explained y-variance in the SOC model, however, was decreasing successively with decreasing spectral resolution, while overfitting increased (Fig. 6-C1 to C3). Only the models based on the hyperspectral resolutions were able to reproduce the comparable complex settings of the relationship between LWIR spectra and SOC content for a successful quantification. Prediction accuracy and precision for the LWIR hyperspectral TASI-resolution were marginally lower than from the full spectral resolution for the soil texture properties, and more pronounced in the accuracy for the prediction of the SOC content (R^2_{SOC} (TASI): 0.733; R^2_{SOC} (full resolution): 0.778).

The low predictability and high complexity of the texture models using the VNIR-SWIR wavelengths were repeated for the models based using HyMap-resolution. The multispectral ASTER-resolution showed low ability for the prediction of the texture properties (Fig. 6-D3 and E3). The prediction of the SOC content using the VNIR-SWIR wavelengths could be realized on a constant level from the full resolution down to the multispectral $ASTER_{VNIR-SWIR}$-resolution with explaining y-variances of about 60% (Fig. 6-F1 to F3).

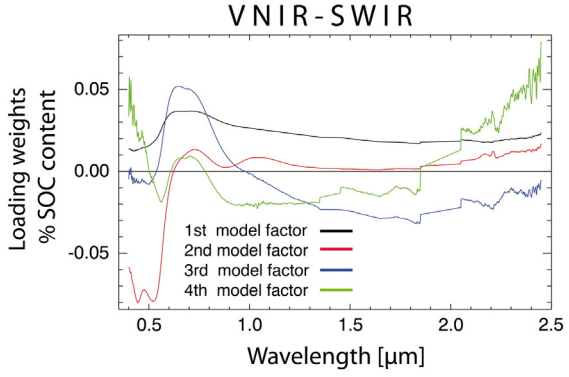

Fig. 8. Loading weights (1–4) of the 4-factor PLS-model for prediction of the SOC content (%) from the VNIR-SWIR soil spectra (full spectral resolution).

3.3. Prediction of the soils' geochemistry (SiO_2 and Al_2O_3 content)

Partial Least Squares calibration and cross-validation were accomplished with the LWIR and the VNIR-SWIR spectral signatures for the soils' SiO_2 and Al_2O_3 content. The descriptive statistics of the datasets used are summarized in Table 1, and the PLS-models' performance indicators for the validation stage are summarized in Tables 3, 4, and 5. The models' y-variances are displayed in Fig. 9. The 137 samples used in this dataset represent a broader range of soil characteristics, as they comprise samples distributed over the whole investigation area (including agricultural and non-agricultural soils).

3.3.1. LWIR

Both geochemical properties, SiO_2 content (associated with quartz) and Al_2O_3 content (associated with clay minerals), were predicted

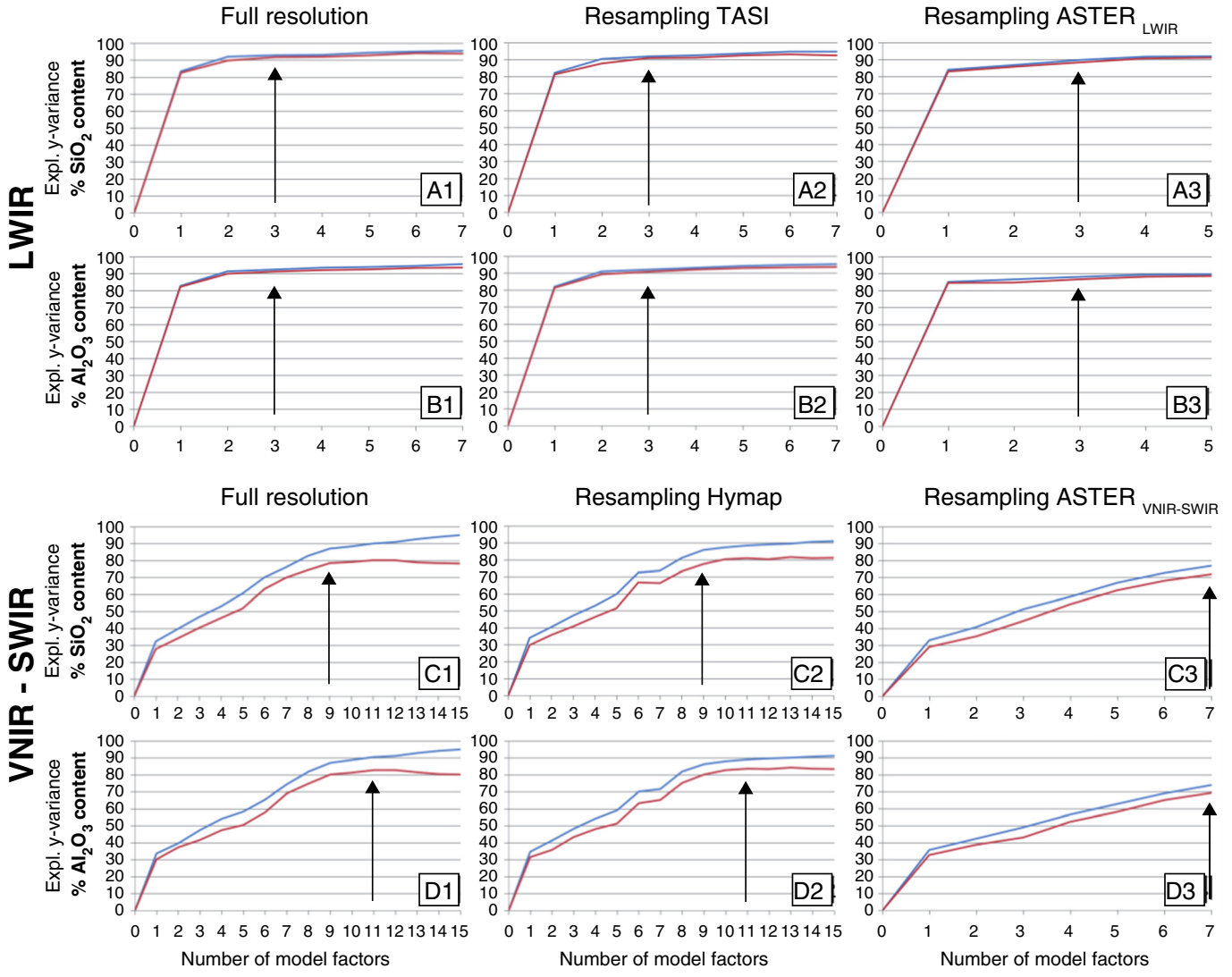

Fig. 9. Explained y-variance of the predicted geo-chemical parameters (SiO_2 and Al_2O_3 content) in the PLS-models based on the LWIR and on the VNIR-SWIR soil spectra in the full spectral resolution and for the spectral resampling. Calibration indicates the blue and cross-validation the red curve. The arrows indicate the number of model factors used in the predictions. (For interpretation of the references to color in this figure legend, the reader is referred to the web version of this article.)

from the full spectral resolution with high accuracy (R^2_{SiO2}: 0.918; R^2_{Al2O3}: 0.911) and high precision ($RMSECV_{SiO2}$: 1.8%; $RMSECV_{Al2O3}$: 0.772%). This performance was accomplished after just 3 factors, with a high degree of robustness (Fig. 9-A1 and B1). This was apparent as small differences in the explained y-variances between calibration and validation. Overfitting was considered negligible in these models.

The RC of the SiO_2-model in Fig. 10 showed the dominant influence of the reststrahlen bands produced by the fundamental molecular vibrations of the Si–O stretching. This can be seen particularly from the ascent between ~8 μm and ~8.6 μm (including the first lobe of the quartz doublet) and the ascent between ~9.3 μm and ~9.8 μm (based on surface scattering). Additionally the importance of the volume scattering induced spectral region from 11 μm on was indicated as indicated in Fig. 3-A2. The RC of the SiO_2–model did also reveal evidence of the spectral feature of features kaolinite at 9.8 μm. The Al_2O_3-model on the other hand was dominated by the spectral features of kaolinite (at 9.0 μm, 9.8 μm, 10.5 μm, and at 10.95 μm) and also showed the influence of the volume scattering region.

The reduction in the spectral dimensionality from the LWIR hyperspectral resolution (full-resolution and TASI) to the multispectral resolution ($ASTER_{LWIR}$) showed only a very small reduction of the prediction indicators for the SiO_2 and the Al_2O_3 content. Five ASTER bands were still sufficient to establish very robust models for both geochemical properties with a high predictive accuracy (R^2_{SiO2}: 0.883; R^2_{Al2O3}: 0.867) and a high predictive precision ($RMSECV_{SiO2}$: 2.15%; $RMSECV_{Al2O3}$: 0.946).

3.3.2. VNIR-SWIR

The simplicity of the LWIR models was in sharp contrast to the very complex VNIR-SWIR models (Fig. 9-C1 and D1). Sufficient prediction from the VNIR-SWIR could only be realized for both geochemical properties by using much more model factors. This is due to SiO_2 having almost no features in the VNIR-SWIR. Due to the fact that the performance indicators do improve in PLS with each additional model factor, the predictive accuracy and the predictive precision from Table 3 were considered as not being meaningful in this case. For the same reason, a detailed interpretation of the RC was not feasible. However, it was noted that compared to the VNIR-SWIR models of the soil properties (sand, clay, and SOC content) these geochemical models did not show such excessive overfitting in the development of the y-variances. Both geochemical VNIR-SWIR models also revealed more influence of the clay mineral feature at 2.16/2.21 μm in their RC. The spectral resampling in

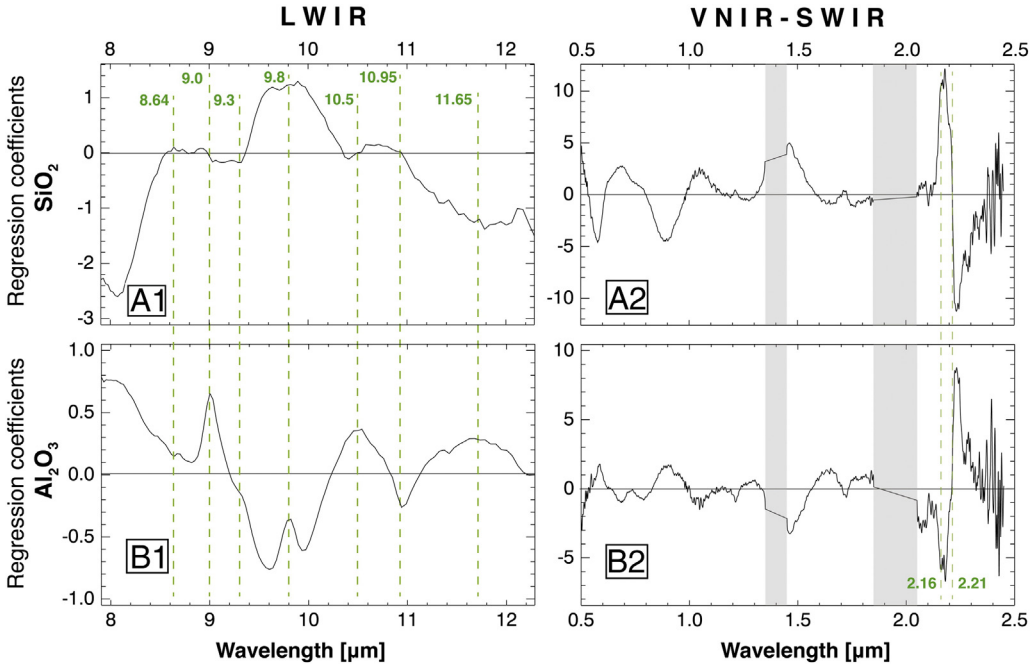

Fig. 10. Regression coefficients (RC) of the PLS-models of the predicted geo-chemical parameters (SiO_2 and Al_2O_3 content) based on the LWIR and based on the VNIR-SWIR soil spectra (full spectral resolution). The dashed green lines indicate wavelength positions of spectral drivers which correspond to identified mineral spectral features (see Fig. 3). VNIR-SWIR-bands which have been ignored in the prediction models due to their proximity to significant atmospheric water-absorption are grayed out. (For interpretation of the references to color in this figure legend, the reader is referred to the web version of this article.)

the VNIR-SWIR showed a decrease in the prediction performance with the transfer from the hyperspectral (HyMap) to the multispectral resolution ($ASTER_{VNIR-SWIR}$) (Fig. 9-C2 to C3 and D2 to D3).

4. Discussion

All of the inspected soil properties (sand-, clay, and SOC-content) and the geochemical properties (SiO_2 and Al_2O_3 content) could be predicted with higher accuracy and precision from the LWIR than from the VNIR-SWIR soil spectra. This difference was particularly evident for the prediction of the soil texture properties, sand and clay content, which possessed a small range in values. Here the VNIR-SWIR was clearly outperformed by the LWIR, as the VNIR-SWIR based models were dominated by the influence of the strong spectral contrast of the iron bearing grain coatings (hematite and goethite) in the VNIR. The texture related spectral feature in the SWIR (2.16/2.21 µm) showed minor influence in these models. This was evident from the models' RC values (Fig. 7). However, the prediction models of the SiO_2 and Al_2O_3 content clearly showed the influence of this spectral feature (Fig. 10-A2 and B2). This could be addressed to either the extended texture range (less conflicting effects throughout grain coatings) or to the fact that this spectral feature is more related to the chemical composition than to the soil texture.

4.1. Spectral requirements for the detection of soil texture

In this study the silt fraction was not considered. In order to determine a soil's texture, its sand (>20 µm) and clay fraction (<2 µm) needs to be known, which allows estimating the complementary silt fraction (2–20 µm). The quantification of the sand and the clay content was basically accomplished from an indicative spectral response from either the particle size or from a distinctive mineralogy within these two fractions. The mineralogy of the sand and the clay fractions generally is sufficiently distinctive. The sand fraction consists predominantly of the mineral quartz, and the clay fraction of clay minerals (e.g. kaolinite). However, the silt fraction typically is a mixture of the mineralogy of the sand and clay fraction (Brady & Weil, 2008). Predicting the silt content was not possible, neither from PLS-models using the LWIR nor from the VNIR-SWIR soil spectra (results are not shown). The reason for the outstandingly successful prediction of the sand and the clay content from the LWIR soil spectra was the presence of both mineralogical and texture-related spectral drivers in these models.

4.2. Modeling texture from VNIR-SWIR despite the influence of iron bearing grain coatings

The models based on the VNIR-SWIR soil signatures, which were still moderately able to predict the soil texture properties (this could only be realized from the hyperspectral resolution), could be explained by the potential relationship between the VNIR-SWIR soil spectra and the soils' texture. Despite the VNIR-dominance of the iron bearing minerals in the investigated soils, the content of hematite and goethite was assessed as low in the XRD analyses. These iron oxides/oxyhydroxides were concentrated in the soils' thin grain coatings. The specific surface rapidly increases with decreasing particle size, which justified an indirect relationship between soil texture and the spectral characteristics of these minerals. This indirect relationship becomes even more complicated by the different spectral characteristics of hematite, goethite, and its mixtures. The PLS models had to consider these circumstances, and thus needed more model factors. This resulted in more complex and less robust models.

4.3. Iron and clay bearing grain coatings in the LWIR and in the VNIR-SWIR

The strong spectral contrast of the hematite and/or goethite in the soils' grain coatings was accounted as the main interference factor that negatively influenced the prediction models based on the VNIR-SWIR. In this regard, the advantage of the LWIR became particularly evident in the prediction of the soils' geo-chemistry. The SiO_2 and Al_2O_3 content, derived from the XRF analyses, is related to the finely ground soil samples (grain size < 20 µm), where the iron bearing minerals of these thin layers cease to significantly influence within the net volume. However, these prediction models were based on the LWIR spectral signatures using the original soil samples, which clearly demonstrated the

existence of hematite and/or goethite in their grain coatings in the corresponding VNIR soil spectra. The high accuracy and the high precision, which were achieved in the prediction of the SiO_2 and Al_2O_3 content (even by using just 5 bands based on the ASTER-resampling), suggest that the LWIR response did not become affected by the soils' grain coatings of hematite and/or goethite. This was because these comparable long wavelengths did not hold enough energy to interact with these oxides/oxyhydroxides (electronic transitions occur at shorter wavelength). Thus, these iron-bearing minerals within the grain coatings appeared transparent for the LWIR.

In contrast, the kaolinite within the grain coatings interacted with both wavelength regions. This was apparent by the presence of strong kaolinite spectral features of the coarse textured soil samples in the VNIR-SWIR and in the LWIR.

The advantage of the LWIR over the VNIR-SWIR was based on the increasing influence of the volume scattering in the LWIR soil spectra with the increasing influence of clay-sized particles, which modified the surface scattering induced features at 10.95 μm with respect to soil texture.

The multivariate data analyses technique, which was used to quantify the soil texture properties, was able to handle these relationships. It involved the whole continuum of the spectrum and as well assisted the spectral interpretation of the models, which confirmed such relationships. Mono-causal quantification approaches, such as from CRAD, were not able to encompass such complex relationships. Hewson, Cudahy, Jones, and Thomas (2012) addressed limitations in the quantification of clay content from spectral indices based on selected wavelengths derived from LWIR soil spectra to interferences from clay mineral particle coatings over coarser grain particles.

4.4. Transferability of the prediction models to soils from other locations

Strictly, the demonstrated PLS models' prediction accuracy/precision are site specific. Increasing deviation or even inefficacy needs to be expected when applying these models to other sites, which show soil characteristics departing from those used in the primary calibration. Similar soil mineralogy and range of the soil properties would increase the feasibility to transfer a model to another site. However, best prediction performance will be achieved using site-specific models, which preferably encompasses the full range of soil characteristics in the calibration stage.

4.5. Soil surfaces under outdoor/field conditions

With regard to an applicability of the laboratory LWIR soil spectra to outdoor/field measurements Salisbury et al., 1994 & Johnson, Lucey, Horton, & Winter, 1998 indicated possible modifications of the soil spectral signatures, as a consequence of the distortion of the pristine soil surface conditions, as well as through the transport, and thus mixture, of such soil samples. Accordingly, an undisturbed soil surface is comparably free of small particles due to atmospheric forces, such as wind and water. These pristine conditions are referred to as *clean soils* and can only be observed in the field. Due to distortion and transport/mixture, these soils get contaminated by small sized particles, such as clay, which surround the soils' grains like coatings (*dirty soils*). As a consequence these *dirty soils* show reduced spectral contrast in their LWIR signatures.

The theory of *dirty* and *clean soils* was tested for pristine soil surfaces in the investigation area during a field survey in April 2011 (Eisele, 2014). Field spectral measurements included agricultural and non-agricultural plots close to the locations from 2010 measured with μFTIR-102 spectrometer (integration time: 16 scans or ~5 s). The spectra were taken under dry soil conditions without noticeable amount of vegetation residues in the FOV. Based on these spectra the theory of *dirty* and *clean soils* could generally be confirmed for non-agricultural (natural) soil surfaces, especially for those which exhibited soil crusts. For the agricultural plots, however, the differences between field and the laboratory spectrum were small. This was attributed to the land management practices on the agricultural plots, which cannot be completely avoided even under conservational farming practices. Fig. 11 demonstrates the difference between the spectra for an agricultural plot (A) and for a non-agricultural plot with a soil crust (B). The locations of these plots are marked in Fig. 1 (A in the lower and B in the upper window).

4.6. Influence of cellulose

Although the paddocks of Mullewa are partially covered with crop residuals due to conservation farming practices, in this study we did not consider the influence of cellulose on the LWIR soil spectra. The quantification of soil properties within the VNIR-SWIR, such as associated with clay content, is in the vicinity of the cellulose feature at 2.08 μm and is potentially affected from its influence (Rodger & Cudahy, 2009). Although cellulose also exhibits spectral features in the LWIR (Elvidge, 1988), we expect less influence from it on the soil spectra than in the VNIR-SWIR. This is a result of the strong spectral contrast of the quartz-based soils, the availability of a greater variety of mineral spectral features, and of texture related spectral features in the LWIR soil spectra.

4.7. Influence of atmospheric gases

For this study it was assumed that there was negligible atmospheric influence for the laboratory and field spectra, but as shown in Fig. 10 the influence of water vapor towards 8 μm is identifiable. As the distance

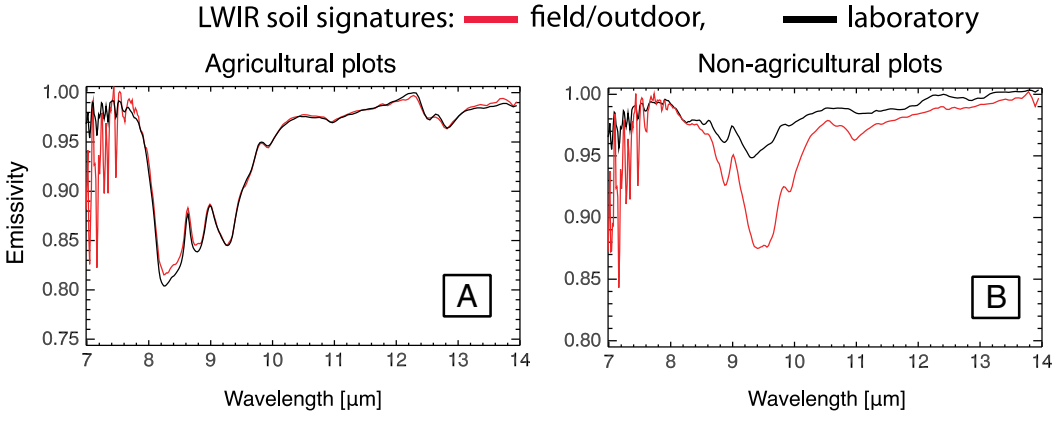

Fig. 11. LWIR soil spectra derived from emission FTIR measurements (μFTIR spectrometer) in the field (red spectra) and in the laboratory (black spectra) for an agricultural plot (A) and for a non-agricultural plot with a surface crust. (For interpretation of the references to color in this figure legend, the reader is referred to the web version of this article.)

Please cite this article as: Eisele, A., et al., Advantages using the thermal infrared (TIR) to detect and quantify semi-arid soil properties, *Remote Sensing of Environment* (2015), http://dx.doi.org/10.1016/j.rse.2015.04.001

from the Earth's surface through remote sensing applications (airborne or spaceborne) increases, there will be a reduction of information from both ends of the atmospheric window due to an increasing atmospheric column between target and sensor (due to $H_2O < 8$ μm and due to $CO_2 > 14$ μm). This could also have an impact on the assumption we made in the TES, for which we defined the spectral range between 7 and 7.5 μm to fit the Planck curve. However, an alternative spectral range could be defined in the vicinity of the second CFF around 12.3 μm. Furthermore, we expect an interference of the soil spectra within the atmospheric window due to the influence of ozone. This would occur in the wavelength region between 9 μm and 10 μm, where important spectral drivers were located (Figs. 7 and 10). The ozone interference would be less influential to airborne hyperspectral imagery than to datasets obtained from spaceborne platforms, which would acquire through the ozone-enriched stratospheric layer.

4.8. Remote sensing perspective

The results demonstrated the LWIR as the appropriate spectral region for an operational remote sensing system to monitor soil surface dynamics in dryland agricultural regions, where small ranges in soil properties and spectral interferences due to grain coatings emerge. In contrast to the VNIR-SWIR, the LWIR did not show noticeable interference with iron based grain coatings (hematite and/or goethite) and compensated for the interference from clay mineral based grain coatings (kaolinite) due to a greater variety of spectral drivers in the LWIR. The soil texture models in the LWIR could benefit from both mineralogical and particle size related spectral drivers.

The spectral resampling showed that the prediction of the soil texture and the geochemical properties could be realized from the multispectral $ASTER_{LWIR}$-resolution data with only slightly decreased accuracy and precision. However, the prediction of the SOC content was not feasible from the multispectral $ASTER_{LWIR}$-resolution. A hyperspectral system would be required for this. We want to emphasize that for a real LWIR multispectral dataset acquired via a remote sensor (e.g. ASTER satellite) we do not expect to obtain such high prediction performance, which was achieved for the soil texture and the geochemical properties and are based on the spectral resampling simulations. Besides the atmospheric influences, a real multispectral dataset would also suffer from a more inaccurate determination of the soils' surface temperature. Note that the spectral resampled laboratory soil signatures contained emissivity values, which were derived via a temperature emissivity separation (TES) approach based on a hyperspectral dimension. A LWIR hyperspectral system would also benefit from the ability to identify the involved soil mineralogy, as these spectral features cannot be resolved with a multispectral resolution. Furthermore a hyperspectral system could deliver important atmospheric information, such as water vapor content.

Some limitations have to be considered with regard to scaling LWIR from laboratory to satellite. LWIR sensors generally rely on coarser spatial and spectral resolution compared to VNIR-SWIR sensors to compensate for less energy in the LWIR. Under-determined solution equations are inevitable for LWIR products. Their accurate interpretation depends predominantly on the accuracy of the TES, which is affected by the SNR of the data and the spectral resolution of the sensor. Especially in mountainous regions high temperature differences can occur due to different slope and aspect that affect the TES in contrast to VNIR-SWIR sensors. However, the inherent self-emission associated with the LWIR allows remote sensing also from shaded targets. Furthermore, LWIR sensors can operate below a cloud cover and even during the night.

5. Conclusion

The study revealed that the LWIR provides the capabilities to detect and quantify small ranges of the soil properties sand-, clay, and SOC-content, as they appear in the semi-arid agricultural landscapes of Mullewa, in Western Australia. Thus, the LWIR offers extended possibilities for potential soil monitoring applications in the area of Mullewa by means of remote sensing. All of the three soil properties and the geochemical properties, SiO_2 and Al_2O_3 content, could be predicted from the LWIR soil spectra with better predictive accuracy and predictive precision than from the VNIR-SWIR soil spectra. From the LWIR spectra, the soil texture and the geochemical properties could be predicted from even a multispectral resolution (spectral resampling to the 5 ASTER LWIR bands) with only a slight loss of performance based on simulation studies.

The findings of this study suggest that the LWIR has the potential to be the ideal wavelength region to quantitatively monitor the soil surface dynamics in semi-arid environments, where small ranges in soil properties occur and spectral interference from grain coatings is possible. This baseline study demonstrated the extended capabilities for a remote sensing of semi-arid environments in the LWIR, as these wavelengths did not show noticeable interference with iron based grain coatings (hematite and/or goethite) and in addition allowed for the compensation for the interference with clay mineral based grain coatings (kaolinite) via a greater variety of spectral features in the LWIR. Based on this study an observation of large scale farming areas, where erosion relevant properties need to be quantitatively derived, appears to be more realistic through the means of a LWIR remote sensing.

Acknowledgments

The authors would like to thank Buddy Wheaton and Dan Carter from the Department of Agriculture and Food of Western Australia (DAFWA), Mike Caccetta (CSIRO), Cindy Ong (CSIRO), and Andrew Hacket (formerly of CSIRO, now BHPB) for the organization and realization of the field survey, and for their numerous suggestions that greatly improved this paper. We would also like to thank Freek van der Meer and the Faculty of Geo-Information Science and Earth Observation (ITC) of the University of Twente for the use of their laboratory environment, the MIDAC system, and their great support. From the GFZ, Rudolf Naumann, Andrea Gottsche, Felix Eckelmann, and Sabrina Herrmann are sincerely thanked for undertaking the XRF and XRD analyses.

References

Baldridge, A. M., Hook, S. J., Grove, C. I., & Rivera, G. (2009). The ASTER Spectral Library Version 2.0. *Remote Sensing of Environment*, *113*, 711–715.

Bartholomeus, H., Epema, G., & Schaepman, M. (2007). Determining iron content in Mediterranean soils in partly vegetated areas, using spectral reflectance and imaging spectroscopy. *International Journal of Applied Earth Observation and Geoinformation*, *9*, 194–203.

Baumgardner, M. F., Silva, L. F., Biehl, L. L., & Stoner, E. R. (1985). Reflectance properties of soil. *Advances in Agronomy*, *38*, 2–44.

Ben-Dor, E., & Banin, A. (1995). Near-infrared analysis as a rapid method to simultaneously evaluate several soil properties. *Soil Science Society of America Journal*, *59*, 364–372.

Ben-Dor, E., Chabrillat, S., Demattê, J. A. M., Taylor, G. R., Hill, J., Whiting, M. L., et al. (2009). Using imaging spectroscopy to study soil properties. *Remote Sensing of Environment, Imaging Spectroscopy Special Issue*, *113*(Supplement 1), S38–S55 http://dx.doi.org/10.1016/j.rse.2008.09.019.

Ben-Dor, E., Inbar, Y., & Chen, Y. (1997). The reflectance spectra of organic matter in the visible near-infrared and short wave infrared region (400–2500 nm) during a controlled decomposition process. *Remote Sensing of Environment*, *61*, 1–15.

Ben-Dor, E., Irons, J. R., & Epema, G. F. (1999). Soil reflectance. In A. N. Rencz (Ed.), *Remote Sensing for the Earth Sciences: Manual of Remote Sensing* (pp. 111–188). Inc.: John Wiley & Sons.

Ben-Dor, E., Taylor, R. G., Hill, J., Dematte, J. A. M., Whiting, M. L., Chabrillat, S., et al. (2008). Imaging spectrometry for soil applications. *Advances in Agronomy*, *97*, 321–392.

Bornemann, L., Welp, G., & Amelung, W. (2010). Particulate organic matter at the field scale: Rapid acquisition using mid-infrared spectroscopy. *Soil Science Society of America Journal*, *74*, 1147–1156.

Bornemann, L., Welp, G., Brodowski, S., Rodionov, A., & Amelung, W. (2008). Rapid assessment of black carbon in soil organic matter using mid-infrared spectroscopy. *Organic Geochemistry*, *39*, 1537–1544.

Brady, N. C., & Weil, R. R. (2008). *The nature and Properties of Soils*. Upper Saddle River, N. J.: Pearson Prentice Hall.

Breunig, F. M., Galvao, L. S., & Formaggio, A. R. (2008). Detection of sandy soil surfaces using ASTER-derived reflectance, emissivity and elevation data: Potential for the identification of land degradation. *International Journal of Remote Sensing*, *29*, 1833–1840http://dx.doi.org/10.1080/01431160701851791.

Breunig, F. M., Galvao, L. S., Formaggio, A. R., & Couto, E. G. (2009). The combined use of reflectance, emissivity and elevation aster/terra data for tropical soil studies. *Revista Brasileira de Ciência do Solo*, *33*, 1785–1794.

Chabrillat, S., Goetz, A. F. H., Krosley, L., & Olsen, H. W. (2002). Use of hyperspectral images in the identification and mapping of expansive clay soils and the role of spatial resolution. *Remote Sensing of Environment*, *82*, 431–445.

Chang, C., & Laird, D. A. (2002). Near-infrared reflectance spectroscopic analysis of soil C and N. *Soil Science*, *167*, 110–116.

Chang, C., Laird, D. A., Mausbach, M. J., & Hurburgh, C. R. (2001). Near-infrared reflectance spectroscopy — Principal components regression analyses of soil properties. *Soil Science Society of America Journal*, *65*, 480–490.

Clark, R. N., Swayze, G. A., Wise, R., Livo, E., Hoefen, T., Kokaly, R., et al. (2007). USGS digital spectral library splib06a. *U.S. Geological Survey, Digital Data Series*, *231*.

Crouvi, O., Ben-Dor, E., Beyth, M., Avigad, D., & Amit, R. (2006). Quantitative mapping of arid alluvial fan surfaces using field spectrometer and hyperspectral remote sensing. *Remote Sensing of Environment*, *104*, 103–117 http://dx.doi.org/10.1016/j.rse.2006.05.004.

Cudahy, T. J., Caccetta, M., Lau, I., Rodger, A., Laukamp, C., & Ong, C. (2012). *Satellite ASTER Geoscience Map of Australia (No. v1), Data Collection.* CSIRO.

Cudahy, T. J., Whitbourn, L. B., Connor, P. M., Mason, P., & Phillips, R. N. (1999). Mapping surface mineralogy and scattering behavior using backscattered reflectance from a hyperspectral midinfrared airborne CO 2 laser system (MIRACO2LAS). *IEEE Transactions on Geoscience and Remote Sensing*, *37*, 2019–2034http://dx.doi.org/10.1109/36.774713.

Eisele, A. (2014). *Möglichkeiten der Nutzung thermal-infraroter Wellenlängen zur fernerkundlichen Erfassung/Quantifizierung von Bodenparametern in semiariden Agrarregionen.* Humboldt-Universität zu Berlin, Mathematisch-Naturwissenschaftliche Fakultät II.

Eisele, A., Lau, I., Hewson, R., Carter, D., Wheaton, B., Ong, C., et al. (2012). Applicability of the thermal infrared spectral region for the prediction of soil properties across semi-arid agricultural landscapes. *Remote Sensing*, *4*, 3265–3286 http://dx.doi.org/10.3390/rs4113265.

Elvidge, C. D. (1988). Thermal infrared reflectance of dry plant materials: 2.5–20.0 μm. *Remote Sensing of Environment*, *26*, 265–285 http://dx.doi.org/10.1016/0034-4257(88)90082-X.

Esbensen, K. H. (2006). *Multivariate Data Analysis in Practice: An Introduction to Multivariate Data Analysis and Experimental Design* (5th ed.). Oslo: Camo.

Gomez, C., Viscarra Rossel, R. A., & McBratney, A. B. (2008). Soil organic carbon prediction by hyperspectral remote sensing and field vis-NIR spectroscopy: An Australian case study. *Geoderma*, *146*, 403–411http://dx.doi.org/10.1016/j.geoderma.2008.06.011.

Haberhauer, G., Rafferty, B., Strebl, F., & Gerzabeck, M. H. (1998). Comparison of the composition of forest soil litter derived from three diff erent sites at various decompositional stages using FTIR spectroscopy. *Geoderma*, *83*, 331–342.

Hecker, C., Dilles, J. H., van der Meijde, M., & van der Meer, F. D. (2012). Thermal infrared spectroscopy and partial least squares regression to determine mineral modes of granitoid rocks. *Geochemistry, Geophysics, Geosystems*, *13*, Q03021http://dx.doi.org/10.1029/2011GC004004.

Hecker, C., Hook, S. J., van der Meijde, M., Bakker, W., van der Werff, H., Wilbrink, H., et al. (2011). Thermal infrared spectrometer for earth science remote sensing applications—Instrument modifications and measurement procedures. *Sensors*, *11*, 10981–10999.

Hecker, C., van der Meijde, M., & van der Meer, F. D. (2010). Thermal infrared spectroscopy on feldspars — Successes, limitations and their implications for remote sensing. *Earth Science Reviews*, *103*, 60–70http://dx.doi.org/10.1016/j.earscirev.2010.07.005.

Hewson, R. D., Cudahy, T. J., Jones, M., & Thomas, M. (2012). Investigations into soil composition and texture using infrared spectroscopy (2–14 μm). *Applied and Environmental Soil Science*, *2012*, 12http://dx.doi.org/10.1155/2012/535646.

Hewson, R. D., Cudahy, T. J., Mizuhiko, S., Ueda, K., & Mauger, A. J. (2005). Seamless geological map generation using ASTER in the Broken Hill-Curnamona province of Australia. *Remote Sensing of Environment, Scientific Results from ASTER*, *99*, 159–172http://dx.doi.org/10.1016/j.rse.2005.04.025.

Hook, S., & Kahle, A. B. (1996). The micro Fourier transform interferometer (mFTIR) — A new field spectrometer for acquisition of infrared data of natural surfaces. *Remote Sensing of Environment*, *56*, 172–181.

Hunt, G. R. (1980). Electromagnetic radiation: The communication link in remote sensing. In B. S. Siegel, & A. R. Gillespie (Eds.), *Remote Sensing in Geology* (pp. 5–45). New York, NY: Wiley.

Hunt, G. R., & Salisbury, J. W. (1970). Visible and near-infrared spectra of minerals and rocks: I. silicate minerals. *Modern Geology*, *1*, 283–300.

Hunt, G. R., Salisbury, J. W., & Lenhoff, C. J. (1971). Visible and near-infrared spectra of minerals and rocks: III. Oxides and hydroxides. *Modern Geology*, *2*, 195–205.

Irons, J. R., Weismiller, R. A., & Petersen, G. W. (1989). Soil reflectance. In G. Asrar (Ed.), *Theory and Applications of Optical Remote Sensing* (1st ed.). New York: Wiley-Interscience (July 3, 1989).

Isbell, R. F. (1996). *The Australian Soil Classification.* Melbourne, Australia: CSIRO Publishing.

Janik, L. J., Merry, R. H., & Skjemstad, J. O. (1998). Can mid infra-red diffuse reflectance analysis replace soil extractions? *Australian Journal of Experimental Agriculture*, *38*, 681–696.

Johnson, R. J., Lucey, P. G., Horton, K. A., & Winter, E. M. (1998). Infrared measurements of pristine and disturbed soils 1. Spectral contrast differences between field and laboratory data. *Remote Sensing of Environment*, *64*, 34–46http://dx.doi.org/10.1016/S0034-4257(97)00166-1.

Karnieli, A., Kidron, G. J., Glaesser, C., & Ben-Dor, E. (1999). Spectral characteristics of cyanobacteria soil crust in semiarid environments. *Remote Sensing of Environment*, *69*, 67–75http://dx.doi.org/10.1016/S0034-4257(98)00110-2.

Kobayashi, C., Kashimura, O., Maruyama, T., Oyanagi, M., Lau, I., Cudahy, T., et al. (2010). Method to reduce green and dry vegetation effects for soil mapping using hyperspectral data. *Presented at the ISPRS Commission VII, Kyoto, Japan.*

Lyon, R. J. (1990). Effects of weathering, desert-varnish, etc., on spectral signatures of mafic, ultramafic and felsic rocks, Leonora, West Australia, with comments on their surface coatings. *Fifth Australian Remote Sensing Conference. Perth WA* (pp. 915–923).

Martens, H., & Naes, T. (1992). *Multivariate Calibration.* John Wiley & Sons.

McCarty, G. W., Reeves, J. B., III, Reeves, V. B., Follett, R., & Kimble, J. M. (2002). Mid-infrared and near-infrared diffuse reflectance spectroscopy for soil carbon measurement. *Soil Science Society of America Journal*, *66*, 640–646.

McKenzie, N., Henderson, B., & McDonald, W. (2002). *Monitoring Soil Change. Principles and Practice for Australian Conditions (Technical Report 18/02).* Canberra, Australia: CSIRO Land and Water.

Mougenot, B., Pouget, M., & Epema, G. F. (1993). Remote sensing of salt affected soils. *Remote Sensing Reviews*, *7*, 241–259http://dx.doi.org/10.1080/02757259309532180.

Mulder, V. L., de Bruin, S., Weyermann, J., Kokaly, R. F., & Schaepman, M. E. (2013). Characterizing regional soil mineral composition using spectroscopy and geostatistics. *Remote Sensing of Environment*, *139*, 415–429http://dx.doi.org/10.1016/j.rse.2013.08.018.

Nanni, M. R., & Demattê, J. A. M. (2006). Spectral reflectance methodology in comparison to traditional soil analysis. *Soil Science Society of America Journal*, *70*, 393http://dx.doi.org/10.2136/sssaj2003.0285.

Nerry, F., Labed, J., & Stoll, M. P. (1990). Spectral properties of land surfaces in the thermal infrared: 1. Laboratory measurements of absolute spectral emissivity signatures. *Journal of Geophysical Research — Solid Earth*, *95*, 7027–7044http://dx.doi.org/10.1029/JB095iB05p07027.

Nicodemus, F. E. (1965). Directional reflectance and emissivity of an opaque surface. *Applied Optics*, *4*, 767–773.

Ninomiya, Y., Fu, B., & Cudahy, T. J. (2005). Detecting lithology with advanced spaceborne thermal emission and reflection radiometer (ASTER) multispectral thermal infrared "radiance-at-sensor" data. *Remote Sensing of Environment, Scientific Results from ASTER*, *99*, 127–139http://dx.doi.org/10.1016/j.rse.2005.06.009.

Notesco, G., Kopačková, V., Rojík, P., Schwartz, G., Livne, I., & Dor, E. B. (2014). Mineral classification of land surface using multispectral LWIR and hyperspectral SWIR remote-sensing data. A case study over the Sokolov Lignite Open-Pit Mines, the Czech Republic. *Remote Sensing*, *6*, 7005–7025http://dx.doi.org/10.3390/rs6087005.

Ribeiro da Luz, B., & Crowley, J. K. (2007). Spectral reflectance and emissivity features of broad leaf plants: Prospects for remote sensing in the thermal infrared (8.0–14.0 μm). *Remote Sensing of Environment*, *109*, 393–405http://dx.doi.org/10.1016/j.rse.2007.01.008.

Rodger, A., & Cudahy, T. (2009). Vegetation corrected continuum depths at 2.20 μm: An approach for hyperspectral sensors. *Remote Sensing of Environment*, *113*, 2243–2257http://dx.doi.org/10.1016/j.rse.2009.06.011.

Rogers, L. G. (1996). Geraldton region: land resources survey. In G. Wilson (Ed.), *Land Resources Series*. Perth, WA: Departement of Agriculture Western Australia.

Rowan, L. C., & Mars, J. C. (2003). Lithologic mapping in the Mountain Pass, California area using advanced spaceborne thermal emission and reflection radiometer (ASTER) data. *Remote Sensing of Environment*, *84*, 350–366http://dx.doi.org/10.1016/S0034-4257(02)00127-X.

Rumpel, C., Janik, L. J., Skjemstad, J. O., & Kogel-Knabner, I. (2001). Quantification of carbon derived from lignite in soils using mid-infrared spectroscopy and partial least squares. *Organic Geochemistry*, *32*, 831–839.

Salisbury, J. W., & D'Aria, D. M. (1992a). Emissivity of terrestrial materials in the 8–14 μm atmospheric window. *Remote Sensing of Environment*, *42*, 83–106.

Salisbury, J. W., & D'Aria, D. M. (1992b). Infrared (8–14 μm) remote sensing of soil particle size. *Remote Sensing of Environment*, *42*, 157–165.

Salisbury, J. W., Hapke, B., & Eastes, J. W. (1987). Usefulness of weak bands in midinfrared remote sensing of particulate planetary surfaces. *Journal of Geophysical Research*, *92*, 702–710.

Salisbury, J. W., & Wald, A. E. (1992). The role of volume scattering in reducing spectral contrast of reststrahlen bands in spectra of powdered minerals. *ICARUS*, *96*, 121–128.

Salisbury, J. W., Wald, A., & D'Aria, D. M. (1994). Thermal-infrared remote sensing and Kirchhoff's law: 1. Laboratory measurements. *Journal of Geophysical Research*, *99*, 11,897–11,911.

Salisbury, J. W., & Walter, L. S. (1989). Thermal infrared (2.5–13.5 μm) spectroscopic remote sensing of igneous rock types on particulate planetary surfaces. *Journal of Geophysical Research*, *94*, 9192–9202.

Salisbury, J. W., Walter, L. S., Vergo, N., & D'Aria, D. M. (1991). *Infrared (2.1–25 μm) Spectra of Minerals.* Baltimore, MD: The Johns Hopkins University Press.

Salvaggio, C., & Miller, C. J. (2001). Comparison of field and laboratory collected midwave and longwave infrared emissivity spectra/data reduction techniques. *Proceedings of the SPIE, Image Exploitation and Target Recognition, Algorithms and Technologies for Multispectral, Hyperspectral, and Ultraspectral Imagery VII. Orlando, Florida, United States of America* (pp. 549–558).

Schlerf, M., Rock, G., Lagueux, P., Ronellenfitsch, F., Gerhards, M., Hoffmann, L., et al. (2012). A hyperspectral thermal infrared imaging instrument for natural resources applications. *Remote Sensing*, *4*, 3995–4009http://dx.doi.org/10.3390/rs4123995.

Sobrino, J. A., Franch, B., Mattar, C., Jiménez-Muñoz, J. C., & Corbari, C. (2012). A method to estimate soil moisture from Airborne Hyperspectral Scanner (AHS) and ASTER data: Application to SEN2FLEX and SEN3EXP campaigns. *Remote Sensing of Environment, Remote Sensing of Urban Environments*, *117*, 415–428http://dx.doi.org/10.1016/j.rse.2011.10.018.

Sobrino, J. A., Mattar, C., Pardo, P., Jimenez-Munoz, J. C., Hook, S. J., Baldridge, A., et al. (2009). Soil emissivity and reflectance spectra measurements. *Applied Optics*, *48*, 3664–3670http://dx.doi.org/10.1364/AO.48.003664.

Solomon, D., Lehmann, J., Kinyangi, J., Liang, B. Q., & Schafer, T. (2005). Carbon K-edge NEXAFS and FTIR-ATR spectroscopic investigation of organic carbon speciation in soils. *Soil Science Society of America Journal*, *69*, 107–119.

Please cite this article as: Eisele, A., et al., Advantages using the thermal infrared (TIR) to detect and quantify semi-arid soil properties, *Remote Sensing of Environment* (2015), http://dx.doi.org/10.1016/j.rse.2015.04.001

Stevens, A., Udelhoven, T., Denis, A., Tychon, B., Lioy, R., Hoffmann, L., et al. (2010). Measuring soil organic carbon in croplands at regional scale using airborne imaging spectroscopy. *Geoderma, Diffuse reflectance spectroscopy in soil science and land resource assessment*, *158*, 32–45http://dx.doi.org/10.1016/j.geoderma.2009.11.032.

Stevens, A., van Wesemael, B., Bartholomeus, H., Rosillon, D., Tychon, B., & Ben-Dor, E. (2008). Laboratory, field and airborne spectroscopy for monitoring organic carbon content in agricultural soils. *Geoderma, Antarctic Soils and Soil Forming Processes in a Changing Environment*, *144*, 395–404http://dx.doi.org/10.1016/j.geoderma.2007.12.009.

Ullah, S., Schlerf, M., Skidmore, A. K., & Hecker, C. (2012). Identifying plant species using mid-wave infrared (2.5–6 μm) and thermal infrared (8–14 μm) emissivity spectra. *Remote Sensing of Environment*, *118*, 95–102http://dx.doi.org/10.1016/j.rse.2011.11.008.

UNCCD (2011). Drylands soil: Sustaining life on earth. *United Nations Convention to Combat Desertification — Transforming Drylands*. United Nations Convention to Combat Desertification.

Viscarra-Rossel, R. A., & Behrens, T. (2010). Using data mining to model and interpret soil diffuse reflectance spectra. *Geoderma, Diffuse reflectance spectroscopy in soil science and land resource assessment*, *158*, 46–54http://dx.doi.org/10.1016/j.geoderma.2009.12.025.

Viscarra-Rossel, R. A., Walvoort, D. J. J., McBratney, A. B., Janik, L. J., & Skjemstad, J. O. (2006). Visible, near infrared, mid infrared or combined diffuse reflectance spectroscopy for simultaneous assessment of various soil properties. *Geoderma*, *131*, 59–75.

Wald, A. E., & Salisbury, J. W. (1995). Thermal infrared directional emissivity of powdered quartz. *Journal of Geophysical Research*, *100*, 24,665–24,675.

Walkley, A., & Black, I. A. (1934). An estimation of the Degtjareff method for determining soil organic matter and a proposed modification of the chromic acid titration method. *Soil Science*, *37*, 29–37.

Whitbourn, L. B., Cudahy, T. J., Huntington, J. F., Connor, P. M., Mason, P., Phillips, R. N., et al. (1997). *Airborne and Laboratory Remote Sensing Applications of the CSIRO CO2 Laser Spectrometer MIRACO2LAS*, *109–118http://dx.doi.org/10.1117/12.277604*.

Wold, S., Sjöström, M., & Eriksson, L. (2001). PLS-regression: a basic tool of chemometrics. *Chemometrics and Intelligent Laboratory Systems, PLS, Methods*, *58*, 109–130http://dx.doi.org/10.1016/S0169-7439(01) (00155-1).

Xiao, J., Shen, Y., Tateishi, R., & Bayaer, W. (2006). Development of topsoil grain size index for monitoring desertification in arid land using remote sensing. *International Journal of Remote Sensing*, *27*, 2411–2422http://dx.doi.org/10.1080/01431160600554363.

Yitagesu, F. A., van der Meer, F., van der Werff, H., & Hecker, C. (2011). Spectral characteristics of clay minerals in the 2.5–14 μm wavelength region. *Applied Clay Science*, *53*, 581–591http://dx.doi.org/10.1016/j.clay.2011.05.007.

Please cite this article as: Eisele, A., et al., Advantages using the thermal infrared (TIR) to detect and quantify semi-arid soil properties, *Remote Sensing of Environment* (2015), http://dx.doi.org/10.1016/j.rse.2015.04.001